

Identification of genes that regulate epithelial cell migration using an siRNA screening approach

Kaylene J. Simpson^{1,3}, Laura M. Selfors¹, James Bui¹, Angela Reynolds², Devin Leake², Anastasia Khvorova² and Joan S. Brugge^{1,4}.

To provide a systematic analysis of genes that regulate epithelial cell migration, we performed a high throughput wound healing screen with MCF-10A breast epithelial cells, using siRNAs targeting 1,081 human genes encoding phosphatases, kinases and proteins predicted to influence cell migration and adhesion. The primary screen identified three categories of hits: those that accelerate, those that inhibit and those that impair migration with associated effects on cell proliferation or metabolism. Extensive validation of all the hits yielded 66 high confidence genes that, when downregulated, either accelerated or impaired migration; 42 of these high confidence genes have not been previously associated with motility or adhesion. Time-lapse video microscopy revealed a broad spectrum of phenotypic changes involving alterations in the extent and nature of disruption of cell–cell adhesion, directionality of motility, cell polarity and shape, and protrusion dynamics. Informatics analysis highlighted three major signalling nodes, β -catenin, $\beta 1$ -integrin and actin, and a large proportion of the genes that accelerated migration impaired cell–cell adhesion.

Cell migration is central to development and tissue remodelling and has a major role in cancer and metastasis. Many genes regulate mammalian cell migration; some are clearly involved in the mechanics of the process, whereas others mediate receptor-driven regulatory pathways. These genes have been identified by targeted investigations or through unbiased genetic screens in *Caenorhabditis elegans* and *Drosophila melanogaster*^{1,2}. The development of small interfering RNA (siRNA) technology has made it feasible to perform genetic screens in mammalian cells.

We used a high throughput siRNA screening approach to identify genes involved in epithelial cell migration, focusing on the generation of a highly validated dataset. This contrasts with the general strategy of selective analysis of a few strong hits with minimal validation of the majority of primary hits^{3–6}. We used an immortalized, non-tumorigenic mammary epithelial cell line, MCF-10A, because of its strong migratory response to EGF, its relative homogeneity, compared with tumour cell lines, and its ability to form an epithelial sheet when confluent. The screen was based on the classical scratch-wound assay⁷. This assay is well recognized for assessing epithelial cell motility. It allows visualization of morphological features and has the potential to identify siRNAs that promote escape from the epithelial sheet, a property associated with tumour-cell dissemination.

Three siRNA libraries were screened; the human phosphatase and kinase libraries were chosen because these enzyme families regulate many cellular pathways. The third, a custom library designed in collaboration with the

Geiger Laboratory (Weizmann Institute, Israel) targeted expanded family members of genes with known or predicted roles in migration or adhesion (migration and adhesion related, MAR).

We identified 34 genes that have a negative regulatory role in migration, 32 that have a positive role and 29 that affected cell metabolism. Forty-two of the high confidence hits have not previously been implicated in cell migration. Informatics analysis implicated many of the hits in cell–cell and cell–matrix adhesion through involvement in β -catenin and $\beta 1$ -integrin pathways, regulation of the actin cytoskeleton and EGFR signalling. This screen provides a resource of high confidence data, annotated at the level of migration effects, cell morphology features, patterns of motility over time and pathway interactions. A fully interactive database is hosted by the Cell Migration Consortium (www.cellmigration.org/pubs/wound_rnai.htm).

RESULTS

Screen overview

To screen for motility in high throughput, we developed a robotic-driven pin to deliver a precise scratch in confluent cell monolayers. The assay conditions were established using siRNAs targeting *RHOA* and *RAC1* (refs 8, 9) and wound healing was evaluated after 12 h when the mock-transfected cells, migrating collectively as an epithelial cell sheet, close the wound by 50–60% (Fig. 1; Supplementary Information, Fig. S1a). The extent of motility, termed the ‘area score’, was numerically quantified and a visual evaluation was also performed to provide a secondary

¹Department of Cell Biology, Harvard Medical School, Boston, Massachusetts, 02115. ²Dharmacon, Thermo Fisher Scientific, Colorado, 80026, USA. ³Current address: The Peter MacCallum Cancer Institute, Smorgon Family Building, St Andrews Place, East Melbourne 3002, Victoria, Australia

⁴Correspondence should be addressed to J.S.B. (e-mail joan_brugge@hms.harvard.edu)

Received 21 April 2008; accepted 1 July 2008; published online 10 August 2008; DOI: 10.1038/ncb1762

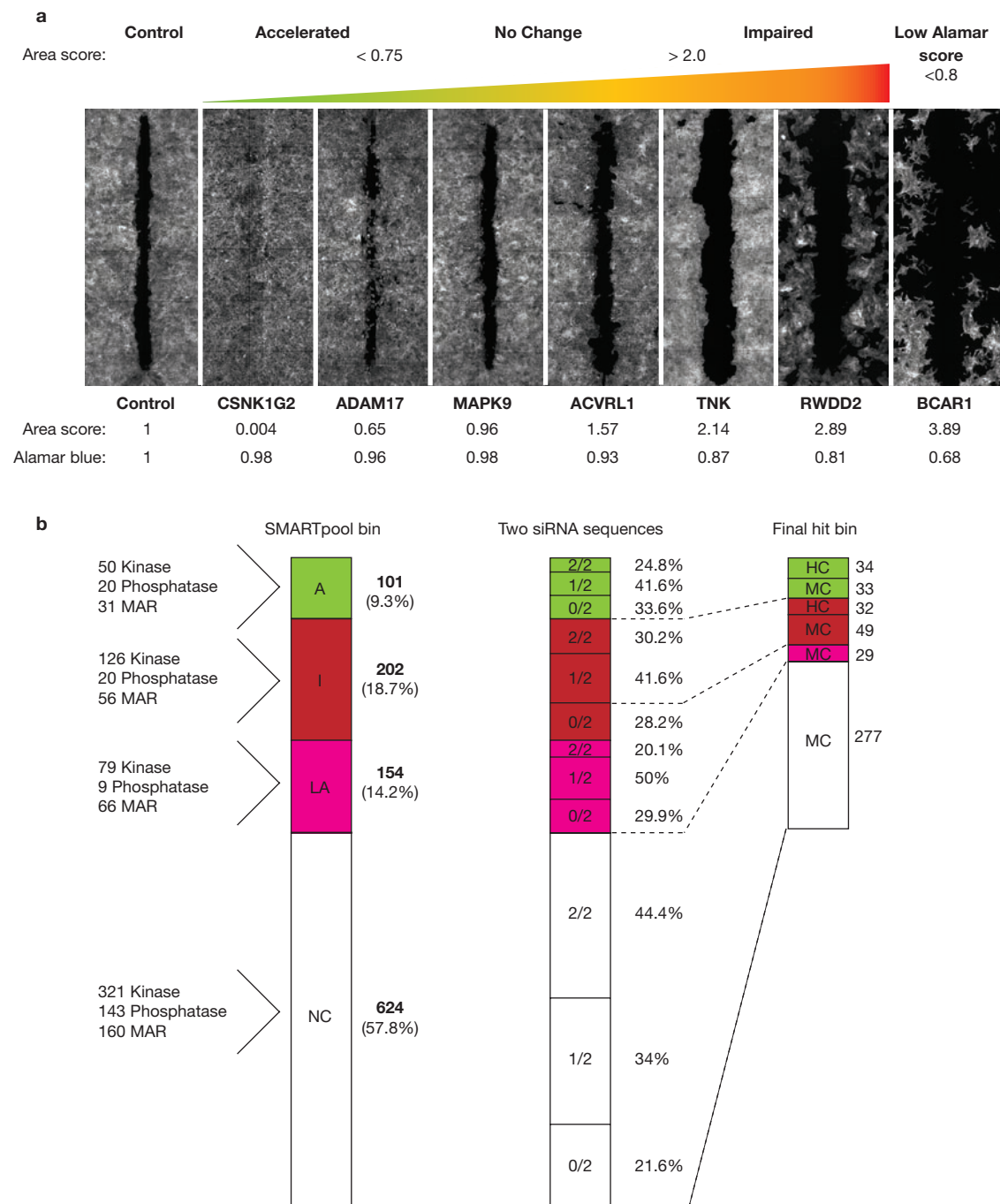


Figure 1 Summary of the wound healing phenotypes and schematic representation of the results from the SMARTpool screen and validation studies. **(a)** Representative wound healing images indicate the continuum of phenotypes, together with the normalized wound area and Alamar Blue scores. siRNAs were binned on the basis of the area score, visual score and Alamar Blue score. Accelerated bin (green) had an area score of <0.75 and visually was considered closed or closing. Impaired bin (red) had an area score of >2.0 and no effect on metabolism (Alamar Blue score >0.8). Low Alamar bin had poor Alamar Blue reduction (<0.8) and generally disrupted monolayer integrity. siRNAs that induced numerical scores bordering the cut-offs were visually inspected and binned appropriately. On occasion, the numerical score could inaccurately reflect wound closure due to small tears in the monolayer, variations in cell morphology or cell dissociation. From the SMARTpool screen, 11.8% of the Accelerated bin and 34% of

the Impaired bin scores were visually overridden. The phalloidin channel montage is shown in grey scale. **(b)** Schematic representation of results from the SMARTpool screen and validation. The left panel: collation of hits for the entire library. The contribution of each siRNA library to each hit bin given in absolute numbers. The total number of siRNAs in each hit bin and the relative proportion of the entire screen is shown. A, Accelerated; I, Impaired; LA, Low Alamar; NC, No Change. Middle panel: distribution of the phenotypic concordance of the two individual sequences within each hit bin, expressed as a proportion of the total number of siRNAs in each bin. 2/2 means both sequences were concordant with the SMARTpool, 1/2 means one was concordant and 0/2 means neither was concordant. Right panel: final hit distribution. High confidence (HC, 3/4 or 4/4 and OTP validation) and moderate confidence (MC, 2/2 or 2/4). siRNAs are indicated by absolute numbers.

assessment of motility. To assess cytotoxicity or reduction in cell number, we measured cellular reducing activity using Alamar Blue immediately before wounding.

The phosphatase library targeted 192 genes, the kinase library targeted 576 protein and phosphotidylinositol kinases and the MAR library targeted 313 genes (Supplementary Information, Table S1a–c). The screen schema is outlined in Supplementary Information, Fig. S1c. Using both SMARTpool siRNA reagents (herein termed SMARTpool) and two individual siRNAs for the primary screen, the siRNAs were classified into hit categories on the basis of migration-specific phenotypes. Detailed validation included screening four individual sequences, quantification of gene knockdown and addressing potential off-target effects. All hits were also re-screened in an additional cell line. Subsequent analysis included examination of cell morphology and time-lapse video microscopy. Bioinformatics analysis was performed to evaluate the coupling of the genes into pathways or networks.

Primary siRNA screen

The continuum of wound healing phenotypes and the numerical cut-off value for classification of each hit bin is shown in Fig. 1a. Representative images of the wound region and cell morphology for each SMARTpool-transfected cell population are shown online (www.cellmigration.org/pubs/wound_rnai.htm). One hundred and one SMARTpools induced an Accelerated migration phenotype (9.3% of total), 202 Impaired (18.7%) and 154 Low Alamar (14.2%; Fig. 1b). Contribution of each library to the hit bins varied but only the kinase and MAR libraries showed significant enrichment of migration hits ($P = 0.02$ and $P = 0.005$, respectively; Supplementary Information, Fig. S2a, b).

In addition to the SMARTpools, we initially screened two of the four individual siRNAs from each pool. This provided a preliminary assessment of the validity of the SMARTpool screen and focused subsequent validation strategies. Scoring for phenotypic agreement with the SMARTpool, siRNAs targeting 394 genes (36.4%) showed consensus with the SMARTpools for both siRNAs: 415 (38.4%) had one concordant siRNA and 272 (25.2%) no concordance (Fig. 1b; Supplementary Information, Table S2a–c).

Evaluation of SMARTpool siRNA efficacy by knockdown

Limited data exists for analysis of gene knockdown under siRNA screening conditions. Using branched DNA (bDNA) technology, we evaluated knockdown before wounding for most of the kinase and phosphatase genes. We found that 42% of the SMARTpools (321) downregulated their target genes by more than 70% (see www.cellmigration.org/pubs/wound_rnai.htm for details). The average knockdown was $67.8 \pm 22.3\%$ (mean \pm s.d., $n = 762$) and did not differ between any hit bin, indicating that the siRNA targeting was effective regardless of the phenotype (Supplementary Information, Fig. S2c, d). The knockdown data was valuable for an overall perspective of the siRNA reagent efficiency under screening conditions; however, the level required to detect a phenotype depends on the target gene, the complexity of the phenotype and sensitivity of the assay¹⁰. As this screen followed a complex phenotype without optimization for individual genes, we have used this data as supportive information relating to the ability of the siRNA to target the gene, and not the primary criteria to define confidence in a particular siRNA.

Validation of siRNAs from the Accelerated and Impaired bins

Focusing in greatest detail on the Accelerated migration bin, we screened all four individual siRNAs from each SMARTpool three times and scored

for phenotypic concordance. High confidence (HC) siRNAs were defined as those that scored a consensus 3/4 or 4/4 with the SMARTpool and Moderate confidence (MC) siRNAs scored 2/4. Twenty-nine (28.7%) siRNAs scored with HC, 32 (31.6%) scored with MC, 31 scored 1/4 and nine scored 0/4 (Fig. 1b; Table 1; Supplementary Information, Table S2a). For the 20 HC siRNAs that scored 3/4, the outlier sequence had no effect. Each of the phenotypic concordance subgroups from the initial screen of two siRNAs gave rise to HC and MC genes (Fig. 1b), with most of the HC hits derived from the 2/2 bin. However, excluding the 0/2 siRNAs would have ignored validated hits, thus screening four individual sequences is optimal for identifying HC hits.

A similar approach was taken for the Impaired migration bin. However, because of limited siRNA availability, we performed a single screen of all four siRNAs from the SMARTpools that scored 1/2 or 2/2 in the initial screen. Thirty-two siRNAs validated with HC (15.8% of the Impaired bin), 48 (23.8%) with MC, 45 scored 1/4 and 20 scored 0/4 (Fig. 1b; Table 1; Supplementary Information, Table S2b). The siRNAs that scored 2/2 from the Low Alamar bin were designated as MC (Fig. 1b). The individual siRNAs that validated and associated sequence information are indicated online (www.cellmigration.org/pubs/wound_rnai.htm).

The Impaired migration phenotype was most prevalent in the SMARTpool screen, probably because of the complexity of the migration process and the possibility that non-specific toxicity can negatively affect migration. However, validation of the Accelerated bin produced a significantly higher proportion of HC genes, compared with the Impaired bin (28.7% versus 15.8%, $P = 0.008$).

Addressing potential off-target effects

Off-target effects are inherent to siRNA technology and result from several mechanisms¹¹. To further address the validity of the siRNA hits, we assayed ON-TARGETplus (OTP) SMARTpools, targeting all HC Accelerated bin genes and a small subset of MC genes. OTPs have been shown to reduce off-target effects^{12,13}. Target mRNA knockdown averaged $70.6 \pm 19\%$ (mean \pm s.d., $n = 16$), which is similar to the standard SMARTpools. Twenty-three OTP siRNAs induced accelerated migration, albeit with generally weaker phenotypes (Supplementary Information, Fig. S3), providing further validation of these HC hits. In addition, this analysis upgraded five genes that had previously scored with MC (*CDC2L5*, *DDEF1*, *MYLK*, *NEDD9*, *STK40*). We did not downgrade those genes that failed to show a phenotype because the OTPs had not been optimized for the original screening conditions and further studies are required to confirm negative results.

Knockdown validation of a subset of the Accelerated genes

To address whether mRNA knockdown correlates with phenotype, mRNA levels for all four individual siRNAs were assessed in parallel with wounding. We observed variability in the extent of mRNA downregulation by each siRNA targeting a single gene (Fig. 2a). siRNAs targeting *CTNND1* (4/4), induced consistent morphology and highly efficient knockdown at the mRNA and protein levels (Fig. 2). All sequences for *ACVR1* and *CDH3* induced at least 60% knockdown, with *CDH3* siRNAs targeting the protein efficiently (Fig. 2a, b). All *ADCK4* siRNAs accelerated migration and altered morphology, but three targeted less than 60%. Although this questions the validity of the phenotype, additional reagents targeting *ADCK4* (OTP and two shRNA vectors (see Supplementary Information, Discussion)) also accelerated migration, suggesting that the effects are on-target (Fig. 2c).

Table 1 Classification of the HC Accelerated and Impaired genes

Symbol	Alias	GO	Time-lapse migration phenotype
Accelerated migration bin			
CDH3	P-cadherin	Adhesion	
CTNND1	p120-catenin	Migration, adhesion	A: minimal adhesion, front–rear polarity
DOCK6	ZIR1		B: transient adhesion, front–rear polarity
PRKACA	PKACA	Migration	
ADCK4	COQ8		
CDC14C	CDC14B2		
CSNK1E	CK1e		
CSNK1G2	CK1g2		
DDEF1	ASAP1	Migration	
GJA1	CX43		
NEK8	NEK12A		C: minimal adhesion, erratic migration, poor or non-existent front–rear polarity
PFN2	Profilin		
PPP1R1B	DARPP32		
PRKCH	PKC-ε		
STK40	SHIK		
STYXL1	DUSP24		
TPD52L3	NYD-SP25		
CDC2L5	CHED		
DUSP18	DUSP20	Adhesion	
FMN1	Formin	Migration	D: adhesive, large protrusions
MYLK	MLCK		
PTPRO	PTPU2		
SRPK2	SFRSK2		
ADAM17	TACE		E: adhesive, collective, medium protrusions
ADCK1	TYK1		
LTK	CASL	Migration, adhesion	F: adhesive, collective, small compact cells
NEDD9	Fit4-L	Migration	
VEGFC	WSS	Migration	
NF1	TAF2A		G: not significantly distinguishable from control
TAF1	ARHA	Migration, adhesion	
RHOA			
RIOK2			
CTNNB1	β-catenin	Migration, adhesion	
ACVR1	ALK2	Migration	Unique
Impaired migration bin			
CSNK2A2	CK2A2		A: weak adhesion, erratic migration, unpolarized
PTPN6	SHP1		
DMPK	DM		
VEGFB	VEGFL	Migration	B: dynamic adhesions, vertical migration
CAMK2B	CAM2		
RSU1	RSP-1	Adhesion	C: dynamic adhesion, larger cells
ENPP5			
LOC390975			
ACP5	TRAP		
ARHGAP26	GRAF		
IKBKE	IKKE		
PRKCE	PKCε		
C9ORF98	DDX31		
CDC2L1	p58		
CRK	CRKII	Migration, adhesion	
TLN1	TLN	Migration, adhesion	
LIMS1	PINCH	Migration	E: not significantly distinguishable from control
ALS2CR2	PAPK		
DUSP6	MKP3		
EPHB2	DRT		
PIK3R5	p101-P13K		
SGK3	CISK		
FLJ25006			
MAP3K11	MLK3		
NRP1	NRPP	Migration, adhesion	E: not significantly distinguishable from control (larger cells)
VIM	Vimentin	Migration	
IGF1R	CD221		
ITGB1	CD29	Migration, adhesion	
AKT1	PKB	Migration	E: not significantly distinguishable from control (very small protrusions)
PHP14	PHP14		
FES	FPS	Adhesion	
ACTB	Actin	Migration	Unique

The siRNAs were binned into subgroups on the basis of time-lapse video microscopy analysis of the migratory patterns. The standard gene symbol is indicated alongside one commonly used alias (from Entrez gene). Gene ontology (GO) terms were defined as cell migration and cell adhesion.

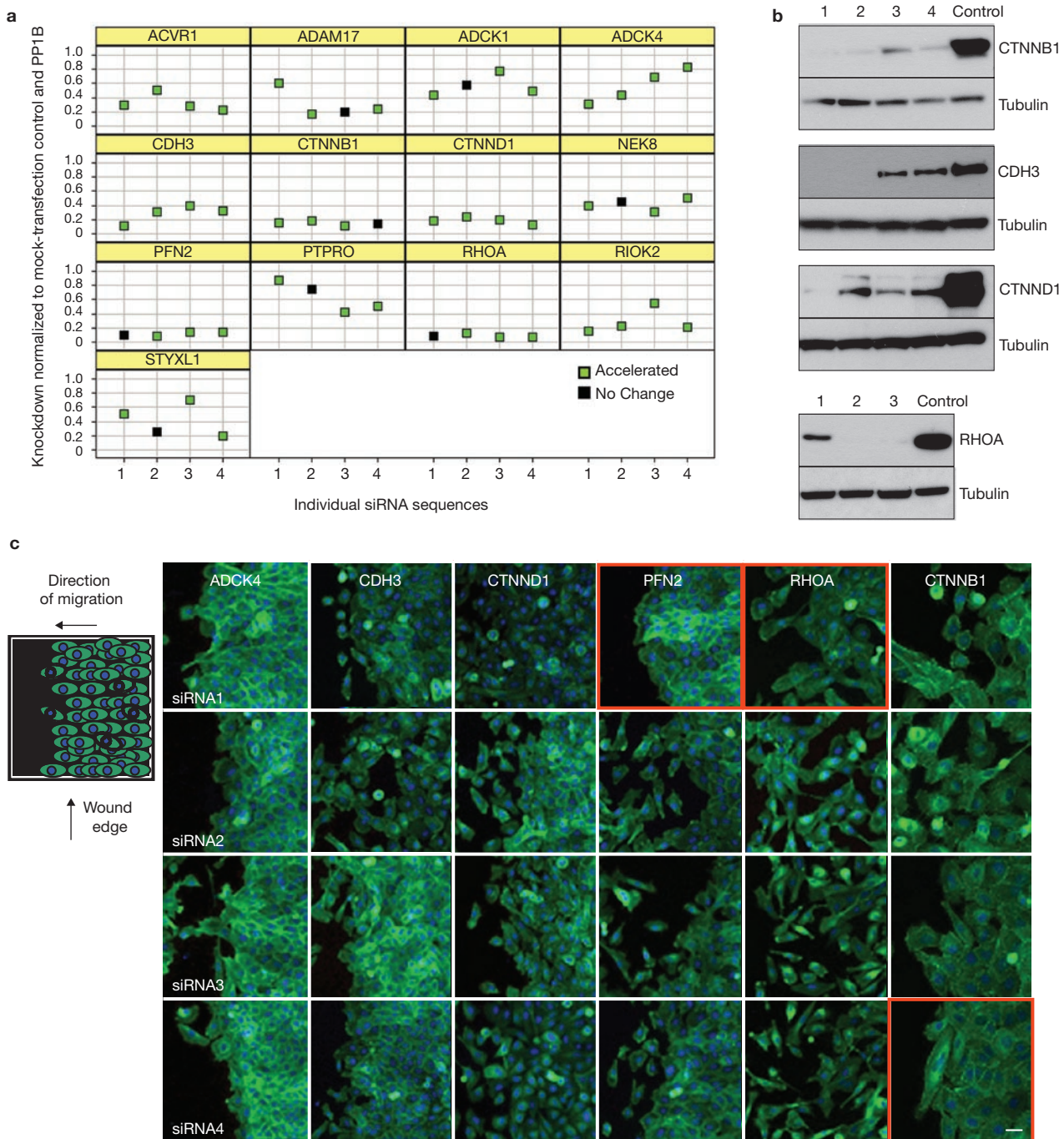


Figure 2 Quantification and correlation of knockdown with phenotype for individual Accelerated bin siRNAs. Four individual siRNAs were transfected and RNA knockdown was quantified using bDNA technology 56 h after transfection, in parallel with wound healing. (a) The trellised box plots show the extent of knockdown for siRNAs 1–4. Accelerated migration is indicated by green and No Change is indicated by black. (b) Analysis of knockdown at the protein level for siRNAs 1–4 for *CTNNB1*, *CDH3*, *CTNND1* and *RHOA*

and corresponding tubulin. Note: *RHOA* siRNA 3 and 4 were duplicated and western blot analysis was performed for siRNA 3 only. Full scans of these blots are shown in Supplementary Information Fig. S8c. (c) Images showing the morphology of cells at the immediate wound edge, stained with phalloidin (green) and DAPI (blue). Cells migrated from right to left as indicated by the schematic diagram on the left. The scale bar represents 25 μ M. siRNAs that induced a No Change phenotype are outlined by a red box.

For the 3/4 HC genes, the non-concordant siRNA targeted the mRNA but did not alter migration (*CTNNB1*, *PFN2*, *RHOA*; Fig. 2). *RHOA* siRNA1 targeted the mRNA efficiently but was less effective at protein knockdown and induced weaker morphological changes. Ineffective protein knockdown may also explain the lack of phenotypic concordance for other siRNAs. Failure of the non-concordant siRNAs to enhance

migration may be due to a suppressive off-target effect that neutralizes increased migration. This seems plausible given that *CTNNB1* and *RHOA* have well documented roles in migration^{14,15} and we have significant experimental validation.

The average knockdown for the HC and MC genes did not differ ($66.5 \pm 21.7\%$ versus $64.3 \pm 20\%$, mean \pm s.d., $n = 13$ and 9, respectively).

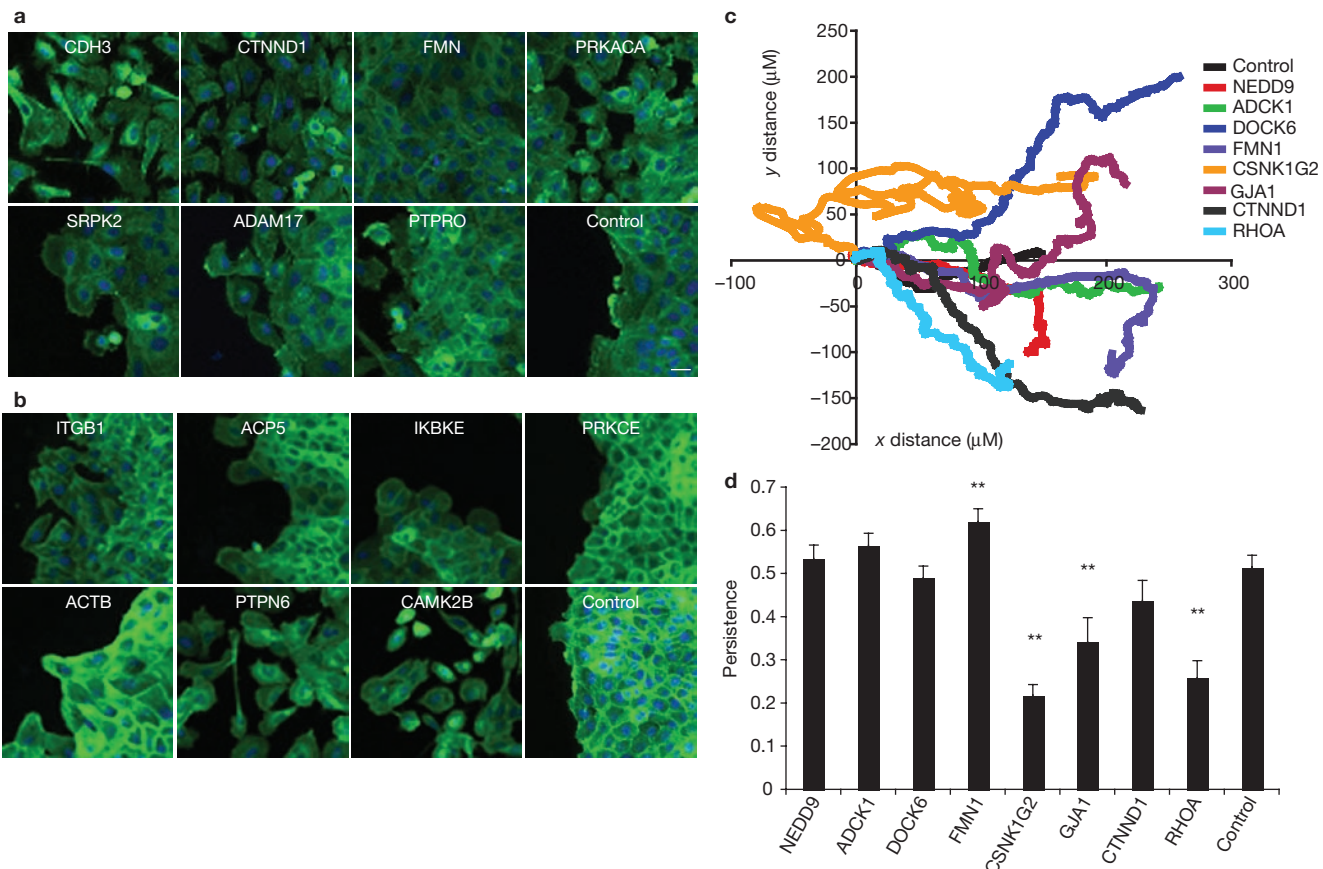


Figure 3 Analysis of cell morphology after transfection with HC Accelerated and Impaired migration siRNAs and quantification of the migration pattern determined by time-lapse imaging. Representative images of cells at the wound edge are shown for selected SMARTpools. (a, b) Accelerated (a) and Impaired (b) bins. Cells migrated from right to left as indicated in Fig. 2c. Phalloidin (green) and DAPI (blue). The scale bar represents 25 μM. The complete set of images is available in Supplementary Information,

However, the MC and 1/4 genes failed to show a correlation between knockdown and phenotype, diminishing our confidence that these effects are on target and suggesting that two concordant siRNAs are insufficient for validation (Supplementary Information, Fig. S4a, b).

Classification of screen results

Integrating the SMARTpool screen with the individual siRNA and OTP validation data, each gene was assigned to a final hit bin: HC (3/4 or 4/4 concordance), MC (2/4 or 2/2 concordance; Fig. 1b) or Discordant (0/4, 1/4, 0/2, 1/2; Supplementary Information, Tables S2a–c). The Discordant siRNAs did not validate with confidence on the basis of differences between the SMARTpool and individual siRNAs, or replicate reproducibility. The siRNAs that induced a No Change phenotype and validated with MC were termed No Phenotype (NP). We identified 66 HC genes that Accelerate and Impair migration and studied these in greater detail (Table 1).

Distinguishing morphological features induced by the HC Accelerated and Impaired genes

We observed a diverse range of morphologies at the wound edge, particularly in the Accelerated bin, with almost two thirds showing significantly altered cell–cell adhesion, ranging from disruption of cell–cell contact at the

wound edge and monolayer, to dissociation only at the wound edge (Fig. 3a; Supplementary Information, Fig. S5a). siRNAs that impaired migration induced limited morphological variability, although several induced some loss of cell–cell contact at the wound edge (Fig. 3b; Supplementary Information, Fig. S5b). Only 3.8% of the Impaired and 1% of the No Change bin showed weak morphological changes.

To investigate the alterations responsible for accelerated or impaired migration, we used time-lapse imaging during wound healing. The videos from this analysis, as well as a progression of cropped static images, and annotation of parameters such as cell morphology, lamellae and lamellipodia protrusion dynamics, speed, direction and the extent of cell–cell adhesion can be found online (www.cellmigration.org/pubs/wound_rnai.htm). The Accelerated genes were divided into seven groups (A–G, with four exceptions that had unique and unclassifiable properties) and the Impaired genes into five groups (A–E, with two exceptions; Table 1; Supplementary Information, Tables S3, S4). A representative from each Accelerated group (indicated by #) was characterized by tracking the migration pattern of eight independent cells (Fig. 4). A selected cell was then graphed to show directionality and persistence (x- and y-axis motility; Fig. 3c). Analyses of persistence indicated that several siRNAs induced highly random motility to close

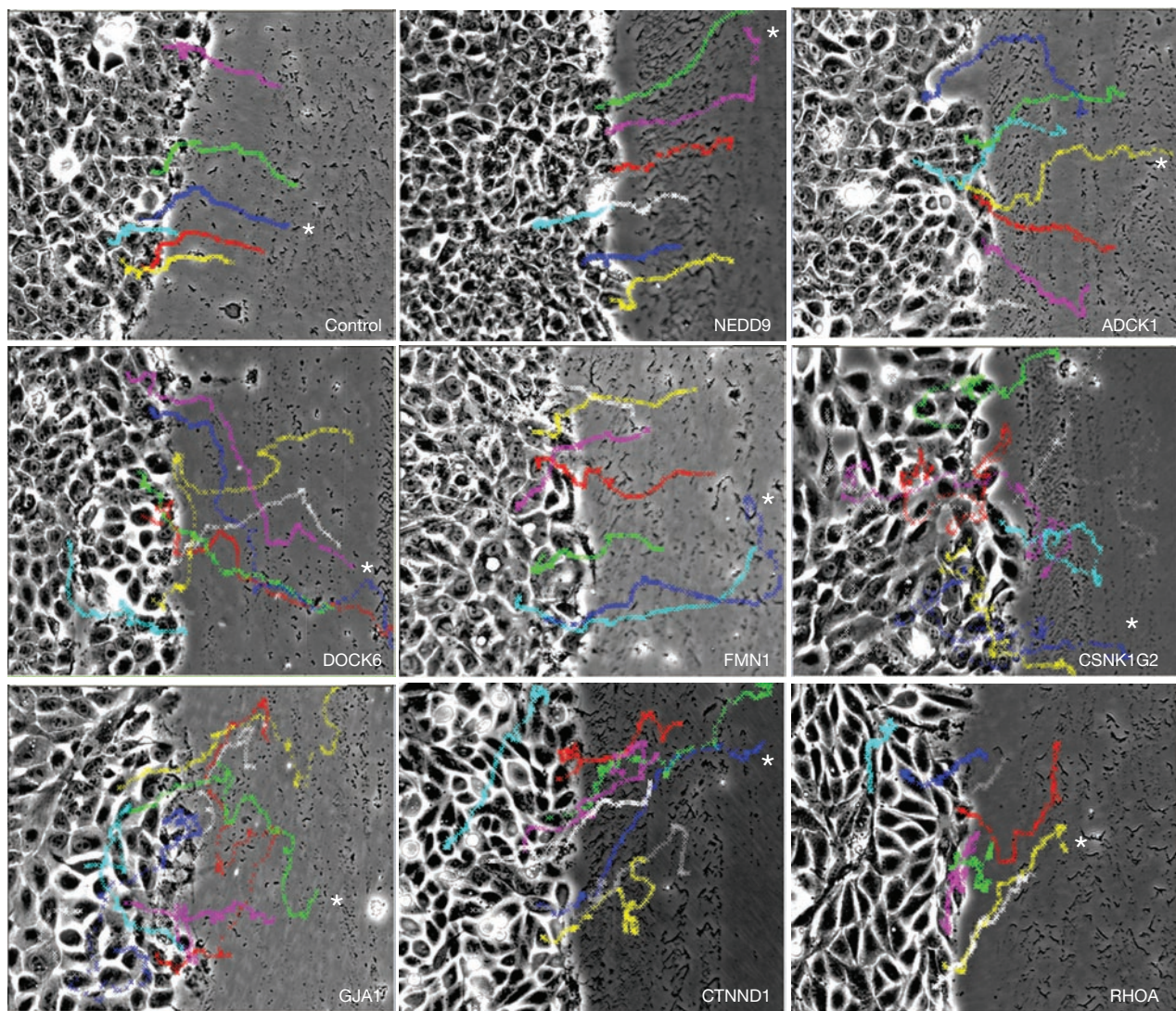


Figure 4 Analysis of the migration pattern of individual cells from representative HC Accelerated migration subgroups determined by time-lapse imaging. The migration paths of eight cells taken from the wound edge and interior monolayer are indicated on an overlay image from the initiation

of imaging. Images were captured every 6 min for 20 h (201 frames). The cell paths annotated by the asterisk correspond to the graphical display of motility in Fig. 3c. Note, some tracks are not easily distinguishable because of contrast.

the wound (Fig. 3d). Images from time-lapse videoes of wound healing assays are shown for selected genes in Figs 5 and 6. The leading edge of a migrating cell can be distinguished as lamellae and lamellipodia using probes specific for cytoskeletal proteins, or electron microscopy¹⁶. However, as we were unable to differentiate these compartments in our time-lapse images, we refer to the dynamic structures at the leading fronts collectively as protrusions.

After wounding, control cells extended small to medium protrusions into the open space. The monolayer was reoriented towards the leading edge and forward movement began approximately 6 h later. The cells polarized, with nuclei localized to the trailing edge and protrusions at the leading front, and maintained contact throughout the migration period.

Cells transfected with Accelerated Groups A, B and C showed significant alterations in cell–cell adhesion and were distinguished by the extent and nature of adhesion impairment, directionality of movement, alterations in cell polarity and leading edge morphologies and dynamics. Within 1 h of wounding, Group A genes (*CDH3*,

CTNND1[#]) induced cell dissociation and rapid, persistent directional migration, with clear front–rear polarity. Group B siRNA transfected cells (*DOCK6*[#], *PRKACA*) showed transient cell–cell adhesions in the monolayer, front–rear polarity and persistent, directional migration, losing adhesion as they filled the wound. Cells transduced with siRNAs targeting Group C, comprising 13 genes (*ADCK4*, *CDC14C*, *CSNK1E*, *CSNK1G2*[#], *DDEF1*, *GJA1*[#], *NEK8*, *PPP1R1B*, *PRKCH*, *STK40*, *STXYL1*, *TPD52L3*) showed minimal cell–cell adhesion, rapid and very erratic migration and poor front–rear polarity. At wounding, cells were organized as an adherent monolayer that dissociated during closure. Single cells migrated rapidly, changed direction frequently, showed defects in retraction and the formation of large tails, and displayed multiple protrusions per cell. A diverse range of leading edge protrusion features were observed, from quite small (for example, *PPP1R1B*, *STK40*) to narrow and extended (for example, *NEK8*, *PRKCH*) and extremely large and broad (for example, *CSNK1E*, *GJA1*). Imaging of subconfluent MCF-10A cells indicated that single cells move persistently, at

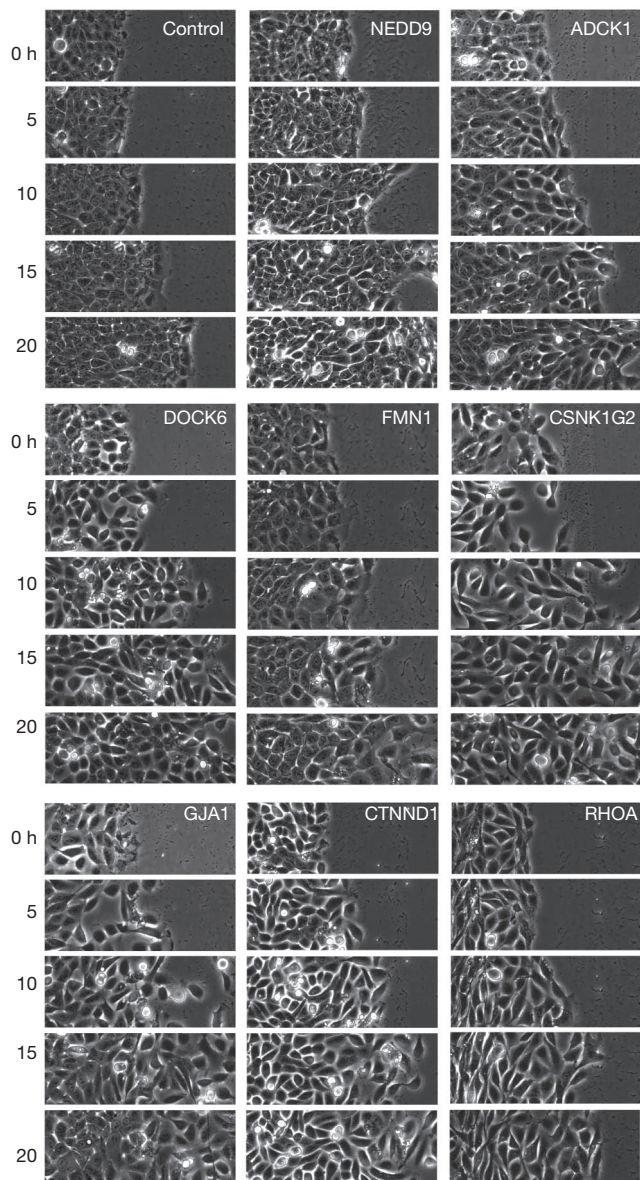


Figure 5 Time-lapse imaging series of cells transfected with representative HC Accelerated migration siRNAs. All fields were cropped at the same position from images collected at 0, 5, 10, 15 and 20 h after the initiation of filming (approximately 45 min post-wounding). Cells were filmed at $\times 20$ magnification.

speeds similar to those seen during wound healing (data not shown). Therefore, the erratic, non-polarized behaviour of dissociated single cells is specific for the knockdown and not a consequence of separation from the monolayer.

Groups D–G siRNA-transduced cells migrated collectively and were distinguished by effects on cell–cell adhesion, morphology of the monolayer and leading-edge cells. Group D (*CDC2L5*, *DUSP18*, *FMN1*[#], *MYLK*, *PTPRO*, *SRPK2*) transduced cells showed large, broad protrusions, especially in leader cells directing migration, and transient cell–cell adhesion. Group E (*ADAM17*, *ADCK1*[#]) cells induced medium-sized protrusions, whereas Group F (*LTK*, *NEDD9*[#], *VEGFC*) cells were distinguished by a compact monolayer. Group G (*TAF1*, *NF1*) cells differed from controls only in speed.

RHOA[#], *RIOK2*, *ACVR1* and *CTNNB1* siRNA-transduced cells showed unique migration patterns. Knockdown of *RHOA* induced elongated, mesenchyme-like cells that maintained minimal adhesion and showed some degree of vertical migration. *RIOK2* knockdown cells polarized with small protrusions, maintained adhesion in the monolayer and moved less erratically than Group C cells. *ACVR1* knockdown cells maintained adhesion and showed a mixture of non-polarized and polarized cells. Knockdown of *CTNNB1* enlarged cell size, slightly disrupted adhesion and provoked some cell death towards the end of the wounding period.

Impaired Group A siRNAs (*CSNK2A2*, *PTPN6*) induced highly motile cells with erratic movement and minimal cell–cell adhesion but failed to move forwards. Group B (*CAMK2B*, *DMPK*, *VEGFB*) siRNAs induced vertical cell movement associated with asymmetric cell–cell adhesion. Group C (*ENPP5*, *LOC390975*, *RSU1*) transduced cells were large, with dynamic cell–cell adhesions, whereas Group D (*ACP5*, *ARHGAP26*, *IKBKE*, *PRKCE*) cells stretched as they moved slowly into the wound. Group E siRNA-transfected cells were morphologically indistinguishable from control cells. *FES* siRNA was unique, causing death of a significant number of cells by the end of the imaging. Loss of *ACTB* almost completely impaired protrusion formation and cells moved forward very slowly with a smooth and united front.

In general, we observed limited protrusion formation in cells transduced with siRNAs that impaired migration, suggesting that these genes affect cytoskeletal rearrangements involved in lamellae/lamellipodial dynamics. In contrast, a broad range of protrusive phenotypes was observed in the Accelerated migration bin. Knockdown of several genes (*PPP1R1B*, *STXYL1*, *STK40*) induced amoeboid-style migration, with cells gliding over the surface, showing limited adhesive connections and small, transient protrusions. This phenotype may reflect a loss of cell–cell adhesion and reduction of cell–substratum adhesion.

Collective migration following a leader cell was observed in both the Accelerated (*LTK*, *NEDD9*, *FMN1*, *MYLK*, *PTPRO*, *SRPK2*) and Impaired (*ARHGAP26*, *C9ORF98*, *CDC2L1*, *IKBKE*, *PRKCE*, *SGK3*, *TLN1*, *FLJ25006*) migration bins; cells oriented after wounding, then progressed into the cleared space behind a defined leader cell that dragged the monolayer in a triangular fashion. Towards closure, the leader cells regressed, or the trailing cells moved forward to form a more uniform edge.

Effect of siRNAs on cell proliferation

To evaluate whether the rate of wound healing was related to effects on cell proliferation, we monitored mitotic events using time-lapse images. There was no correlation between accelerated migration and increased cell proliferation and interestingly, several siRNAs suppressed proliferation (Supplementary Information, Table S3). Many Impaired bin siRNAs decreased the number of mitoses (Supplementary Information, Table S4) but there was no correlation between proliferation and migration distance, suggesting that although reduced proliferation may contribute to the phenotype, other factors are also involved.

Expression of cell adhesion proteins in the HC Accelerated bin.

To investigate the biochemical basis for the variation in cell–cell adhesion, we analysed E-cadherin, P-cadherin and N-cadherin expression (Supplementary Information, Fig. S6a). Knockdown of *CTNNND1*,

CDH3 and *PRKACA* reduced cell–cell contact and total E-cadherin and P-cadherin expression. Interestingly, E-cadherin expression increased in some cell populations with weak cell–cell adhesions (*ADCK4*, *CDC14C*, *CTNNB1*, *CSNK1E*, *DOCK6*, *GJA1*, *PRKCH*, *STYXL1*) and some that maintained contact (*ADAM17*, *DUSP18*, *LTK*, *FMN1*). Upregulation of N-cadherin, characteristic of an epithelial to mesenchymal transition¹⁷, correlated with disruption of cell–cell adhesion (*ADCK4*, *NEK8*, *RIOK2*, *RHOA*, *CDC14C*), but not all, siRNAs (*ADCK1*, *NEDD9*). Downregulation of N-cadherin expression was also observed for several genes that caused cell dissociation (*CTNND1*, *GJA1*, *STK40*; Supplementary Information, Fig. S6a).

Secondary SMARTpool screen

The Low Alamar phenotype could reflect a loss of monolayer integrity caused by loss of cell–cell or cell–substratum adhesion, suppression of cell proliferation, cell death or metabolic impairment. To address whether apoptosis is involved, we screened MCF-10A cells overexpressing the anti-apoptotic protein Bcl-2. The Low Alamar phenotype was rescued for only nine SMARTpools (*MSX1*, *NCAM1*, *RABGEF1*, *SORBS1*, *TGFB3*, *NRCAM*, *PVR*, *PLAUR*, *MAPKAPK2*; Supplementary Information, Table S2c). Of these, the first five impaired migration and the remainder had no effect. Therefore, apoptotic cell death is not the major cause for classification in this bin.

ERBB2 has strong pro-survival activity and allows EGF-independent proliferation of MCF-10A cells^{18,19}. Overexpression of ERBB2 in MCF-10A cells rescued the Low Alamar phenotype induced by the majority of the SMARTpools, including the nine genes rescued by Bcl-2 (139/154; Supplementary Information, Table S2c). Seventeen SMARTpools accelerated and 82 impaired migration, suggesting that ERBB2 overexpression either unmasks migratory phenotypes obscured by toxic effects, or sensitizes MCF-10A cells to loss-of-function effects that can enhance migration (Supplementary Information, Fig. S7a).

The Accelerated and Impaired bin siRNAs were also screened in MCF-10A-ERBB2 cells (Supplementary Information, Table S2a, b). From the Accelerated bin, 83 maintained the phenotype and 18 had no effect. From the Impaired bin, 32 impaired migration, 15 accelerated and nine were Low Alamar (Supplementary Information, Fig. S7b). In summary, screens in ERBB2- and Bcl-2-expressing cells revealed an additional 111 candidate hits that require further validation.

DISCUSSION

We undertook a systematic and stringent screening approach that identified 6.1% of siRNAs as HC regulators of migration and 2.7% that suppressed migration and lowered the cellular reducing potential. This proportion is higher than the hit-rate for a whole genome screen²⁰, possibly owing to the focused nature of our siRNA collection, and scoring multiple phenotypes. Forty-two HC genes have not been previously associated with specific ‘cell migration’ and ‘cell adhesion’ gene ontology (GO) terms (Table 1).

Time-lapse microscopy highlighted the many phenotypes associated with the HC Accelerated and Impaired bins. Many knockdown cells showed transient and highly dynamic cell–cell adhesions, often involving short-lived regions of contact, suggesting that these siRNAs may prevent maturation of stable cell–cell adhesions, potentially by alterations in adherens junction complexes or the linkage of junctional complexes to the cytoskeleton. Alternatively, alterations in cell–matrix adhesions

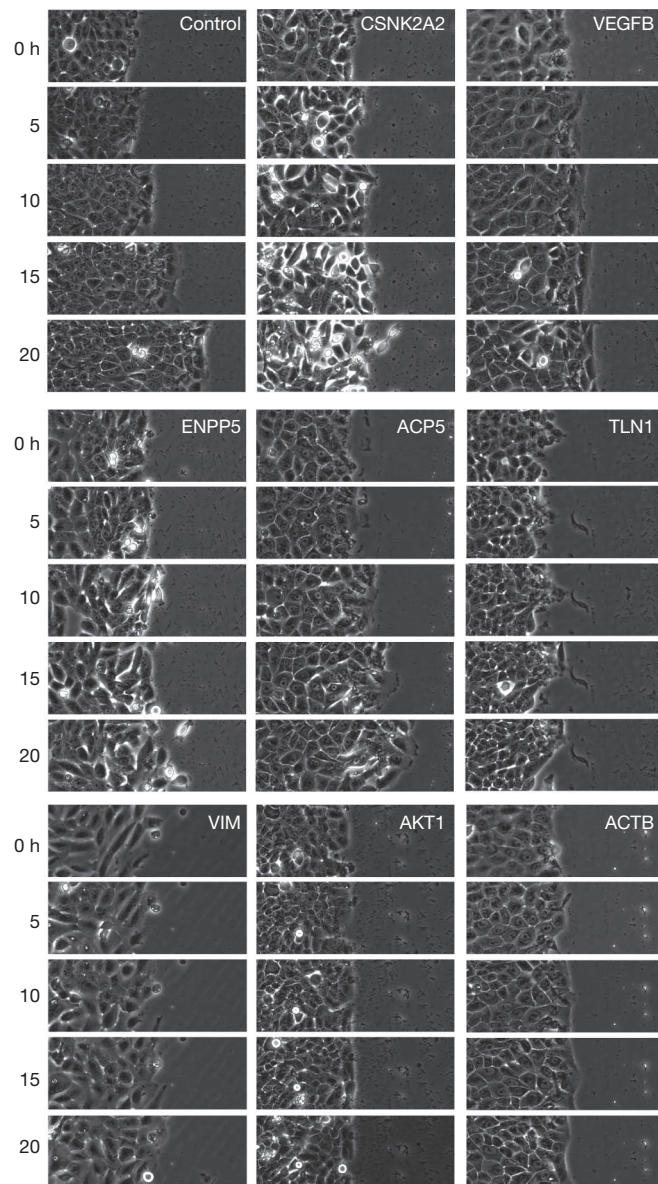


Figure 6 Time-lapse imaging series of cells transfected with representative HC Impaired migration siRNAs. All fields were cropped at the same position from images collected at 0, 5, 10, 15 and 20 h after the initiation of filming (approximately 45 min post-wounding). Cells were filmed at $\times 20$ magnification.

that affect adherens junction dynamics may also weaken cell–cell adhesion²¹. Multiple siRNAs induced defects in cell polarity, causing either complete disruption (protrusions in all directions) or a bipolar phenotype (protrusions at opposing ends). Many siRNAs regulate the dynamics and morphology of protrusions. Although impaired motility was often associated with very small protrusions, this was not universally observed (*PTPN6*, *RSU1*). Conversely, we only observed enlarged protrusions for the Accelerated Group D, which includes *MYLK*, a protein that regulates myosin contraction and has been implicated in regulation of protrusion dynamics. Knockdown of both myosin II isoforms in fibroblasts causes a significant expansion of protrusions, suggesting that the genes in this group may affect actin–myosin contraction²². Several siRNAs (*CSNK1E*, *CSNK1G2*, *GJA1*, *PFN2*, *PRKCH*) induced extensive ruffling at the leading

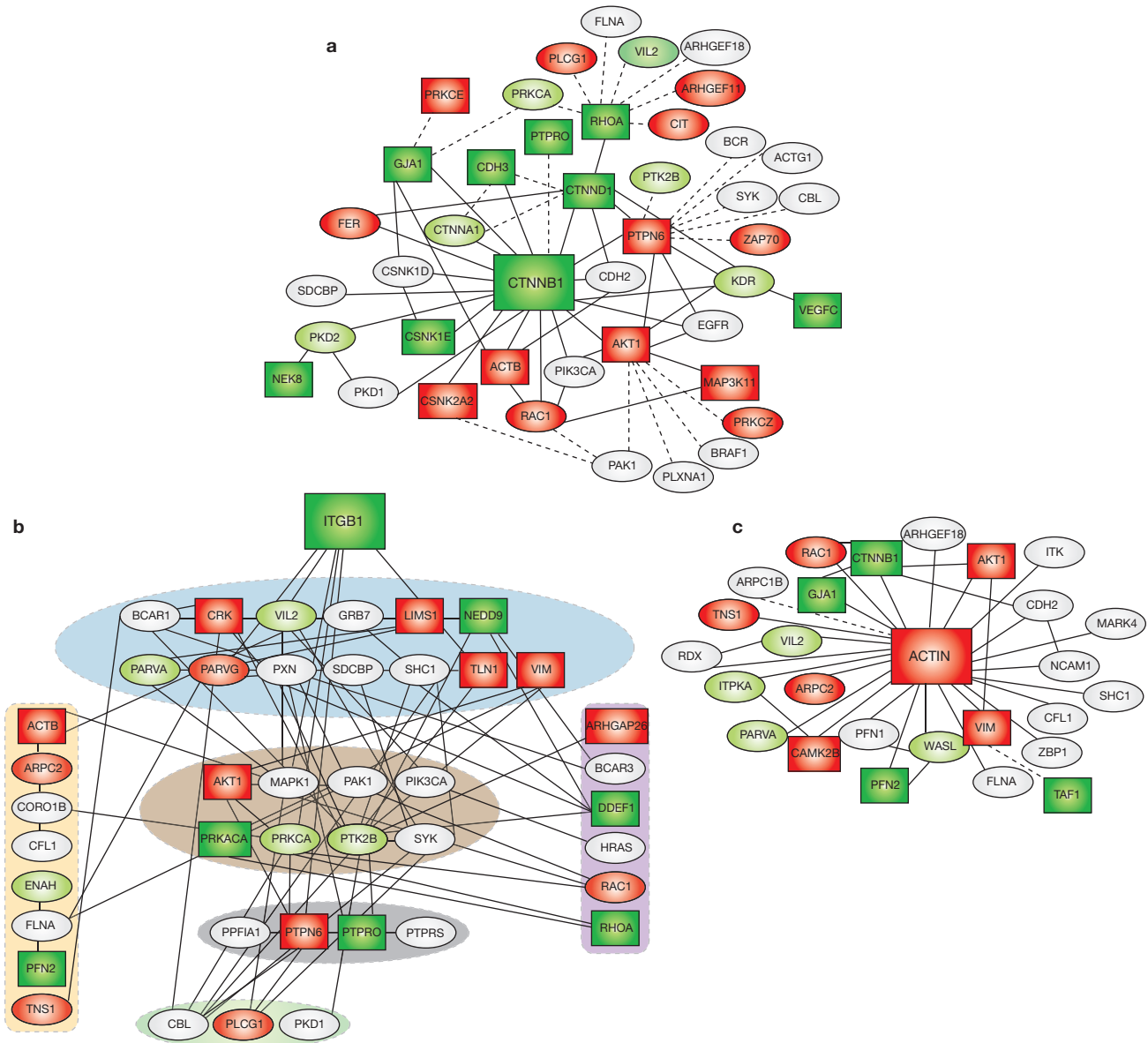


Figure 7 Network relationships for the major signalling nodes β -catenin, β 1-integrin and actin. These networks incorporate siRNAs from the HC and MC Accelerated and Impaired bins and from screening in the ERBB2 background. (a, b) β -catenin network (a) and β 1-integrin network (b). The genes have been classified into GTPases/GTPase regulators (shaded purple), actin regulators (yellow), adaptors (blue), kinases (brown), phosphatases

edge. Impaired group D siRNAs showed compact monolayers at the initiation of wounding that stretched after minimal movement, possibly due to a lack of coupling between the forces at the front and rear of the cell.

The formation of leader cells^{23–26}, shown to involve RHOA regulation of the actin cytoskeleton²³, suggests that the temporal and spatial regulation of RHOA–cytoskeletal signalling is unbalanced by those siRNAs. Knockdown of ACP5, ARHGAP26, CDC2L1, DMPK, NEDD9 and VEGFC induced nuclear rotation, similar to that seen in Swiss 3T3 fibroblasts exposed to mechanical shear stress²⁷ and Rat2 fibroblasts deficient in myosin IIB²². This may be mediated by nuclear lamin A/C through an inability to polarize the microtubule network²⁸, suggesting a role for these genes in MTOC polarization.

(grey) and others (green). (c) Actin. Rectangle: HC (green, Accelerated; red, Impaired); filled oval: MC (green, Accelerated; red, Impaired); unfilled ovals represent genes identified in the ERBB2 background. Solid lines are direct interactions established by Ingenuity and dashed lines represent interactions determined from the following protein–protein interaction databases (BioGrid, HPRD and the Adhesome³⁴).

Most of the siRNAs affecting cell–cell adhesion, polarity, nuclear spinning and protrusion dynamics have no prior association with these processes. To identify pathways that link the HC genes and decipher the role of the 42 previously unknown migration genes, we used Ingenuity software. The top ranking network linked 28 of the 66 genes and centred around β -catenin, β 1-integrin and actin, all of which are known to regulate cell migration. Expansion of these nodes identified extensive networks (Fig. 7a–c) that are discussed in further detail (Supplementary Information, Discussion). Many of the genes that interact with β -catenin accelerated migration and caused dissociation from the epithelial sheet, supporting a role for these genes in regulating cell–cell adhesion. The β 1-integrin network was enriched in genes that impaired migration, including a large number of focal adhesion

proteins. Enrichment of actin-interactive proteins was expected, given their crucial role in regulation of the cytoskeleton. However, only *MYLK* and *MYL5* scored a phenotype. The Low Alamar network revealed a strong bias towards the canonical EGFR/receptor tyrosine kinase signalling pathway (Supplementary Information, Fig. S7c).

Cancer progression is associated with abrogation of normal controls that limit cell migration and invasion, eventually leading to metastasis. These changes typically involve enhanced migration, alteration in adhesion proteins and transient loss of cell–cell contact. We observed such phenotypes in the screen, raising the possibility that many genes may be associated with altered properties of cancer cells (Supplementary Information, Discussion). For example, *CSNK1E* accelerates migration, induces cell dissociation and is expressed at low levels in poorly differentiated, higher-grade tumours²⁹. *RSU1* impaired migration and is selectively upregulated in basal high-grade breast tumours (www.oncomine.org).

This screen identified a large number of genes that positively or negatively regulate cell migration. Although elucidation of the regulatory mechanisms requires additional studies, many of the siRNAs that enhanced cell migration disrupted cell–cell junctions. Focusing on these genes may provide new insights into processes that regulate cell–cell adhesion. Many HC genes have not been previously associated with cell migration and are suitable for analysis. Additional genes that regulate cell migration may be identified through further validation of the MC siRNAs (33 Accelerated, 50 Impaired and 29 Low Alamar). □

METHODS

Screen design. A description of the screen design according to MIARE guidelines (v. 0.6.5) can be found online (www.cellmigration.org/pubs/wound_rnai.htm).

Cell culture, transfection and screening conditions. MCF-10A parental cells and lines overexpressing ERBB2 and Bcl-2 were cultured³⁰ (<http://brugge.med.harvard.edu/protocols>) at a consistent density for a maximum of eight passages. Cells were plated at 8.1×10^3 per well in black-walled 96-well plates (Costar) in antibiotic-free growth medium (Invitrogen) 16 h before transfection. Transfections were performed robotically using a CyBio CyBi-well robot with siRNAs (final concentration 50 or 100 nM) and DharmaFECT 3 transfection reagent (0.18 ml per well; ThermoFisher Scientific) diluted in Optimem (MediaTech). Transfections were performed in duplicate and quadruplicate if knockdown was evaluated.

The effect of transfection on cell metabolism was measured by reduction of Alamar Blue dye (Biosource), a membrane-permeable, non-toxic dye that fluoresces when reduced, reflects cell viability, proliferation and metabolism³¹. The reagent was added 56 h after transfection, to a final concentration of 5%, incubated for 1 h at 37 °C and quantified on a plate reader at 530/590 nm.

Cells were wounded 58 h after transfection by generating a longitudinal scratch (coefficient of variation 3.1%) using a robotically driven (Seiko) stainless-steel pin machined to deliver a scratch of 1.5×4 mm. After wounding, cells were washed once with growth medium and incubated for a further 12 h at 37 °C.

Analysis of wound healing. Cells were fixed (2% paraformaldehyde, 200 mM KCl, 20 mM Pipes pH 6.8, 14% sucrose, 4 mM MgCl₂ and 2 mM EGTA) for 10 min then stained with rhodamine-conjugated phalloidin (Molecular Probes) and DAPI in the presence of 0.2% triton-X-100 in Tris (pH 7.5) for 20 min. The wound was imaged as individual panels and these combined into a montage for visualization of the entire wound, using an Applied Precision CellWorx microscope with a fixed $\times 10$ objective and 1×1 binning. Motility was quantified using a custom-designed MetaExpress (Molecular Devices) journal that used threshold analysis to determine the area remaining after closure. Individual panels were used for higher resolution image analysis by cropping a representative 5-cm-square section from the wound edge followed by 50% compression. Average area scores were calculated (see below) and a blinded visual analysis was performed by two independent investigators.

Time-lapse video microscopy. Transfections were scaled to a 24-well dish format at a final concentration of 50 nM. Cells were wounded 52 h after transfection and imaged using a $\times 20$ ELWD objective on a Nikon TE2000E automated inverted microscope at 37 °C in the presence of CO₂ with the media blanketed by mineral oil (Sigma) to prevent evaporation. Imaging began 45 min after wounding and two fields were taken (either side of the wound) per well at 6 min intervals for 20 h. Migration patterns were followed for eight different cells for representative genes using the manual tool ‘track points’ in MetaMorph. The migration distance was calculated as the sum of the distance moved in each field. Persistence was calculated as a ratio of the net x-axis distance to the total distance moved.

siRNA libraries. All siRNA reagents were obtained from Dharmacon (www.thermo.com/Dharmacon) based on gene annotation from 2004. The complete list of genes, Entrez gene ID and catalogue number can be found in Supplementary Information, Tables S1a–c and online (www.cellmigration.org/pubs/wound_rnai.htm). A subset of genes was selected for off-target analysis using ON-TARGETplus SMARTpools. Focused studies on specific-hit genes were performed by selecting and re-arraying the siRNA into 96-well plates using a Tecan EVO75 Liquid Handler.

Immunoblotting. Transfections were scaled to 6-well dishes at a final concentration of 50 nM. Cells were lysed by scraping into RIPA buffer⁸, proteins (20 mg of total lysate) separated using the Novex precast gel system (Invitrogen), transferred to PVDF membrane (Immobilon), hybridized in 2.5% milk in tris-buffered saline with Tween20 and detected with Pico chemiluminescence reagent (Pierce). Primary antibodies were used at a dilution of 1:1000 and secondary HRP-conjugated mouse or rabbit antibodies (Jackson Laboratories) at 1:5000. E-cadherin (610182), P-cadherin (610228), N-cadherin (610921) and p120-catenin (610134) were purchased from BD Bioscience Pharmingen. β-tubulin (Ab6046, Abcam), RHOA (26C4; Santa Cruz Biotechnology).

shRNA infections. pLKO.1puro-based lentiviral shRNA vectors³² (generously provided by The RNAi Consortium, Broad Institute, MA) were used to downregulate selected hit genes. MCF-10A cells were infected and selected as described³³.

Data analysis and normalization. Data analysis was automated using a custom perl script, which parsed the MetaExpress (wound healing area score) and plate reader (Alamar Blue data) raw data files to generate an Excel spreadsheet with raw values, calculated values and hyperlinks to montaged wound images (see below). PipelinePilot software (Sci-teric) was used to manipulate Excel files and create subdatabases.

The script calculated an area score for each siRNA reagent as follows: to correct for plate-to-plate variability, the area value from each well was normalized to the trimmed mean (20%) of all area values from the plate, excluding positive controls. Fold change relative to the mock-transfected control was calculated by dividing the plate-normalized values by the median of all the normalized mock-transfected controls from all plates on the same screening day. Mean fold changes from replicates were calculated.

During assay optimization, we found that Alamar Blue values showed positional ‘edge’ effects, independent of the siRNA reagent. A correction factor was calculated for each plate by dividing the trimmed mean (20%) of the internal wells by the trimmed mean (20%) of the edge wells. Values from wells positioned at plate edges were multiplied by this correction factor, and plate normalization and fold changes were calculated as for the area score.

For each gene, the perl script generated hyperlinks to image montages created using perlMagick (ImageMagick, <http://www.imagemagick.org/script/perl-magick.php>). The montages contained all wound images for that gene, including replicates and different siRNA reagents, as well as the appropriate plate-specific mock-transfected controls.

Statistical analysis of enrichment was performed using the binomial distribution and simple interactive statistical analysis (SISA, home.clara.net/sisa).

Quantification of knockdown. The level of target gene knockdown was quantified from duplicate plates using branched DNA (bDNA, a nucleic acid hybridization method to directly quantify the amount of mRNA) and the QuantiGene High Volume kit for the direct quantification of cellular mRNA (Panomics) using target specific probes. Values were normalized to an internal PP1B control, averaged and expressed relative to mock-transfection control levels.

Network analysis. Protein interaction networks for the HC gene set were generated using Ingenuity Pathways Analysis (Ingenuity Systems, www.ingenuity.com). The focus genes were overlaid onto a global molecular network developed from direct interactions and sub-networks were algorithmically generated based on their connectivity. To further investigate the sub-networks, each node (β -catenin, $\beta 1$ -integrin, actin) was entered into the program and all direct up and downstream interactors were identified using the Grow Tool. Additional databases (Bind, BioGRid, HPRD) were also used.

Analysis of hits using gene ontology terms. We searched three databases, the Biobase BioKnowledge Library (BKL, <http://www.biobase-international.com/pages/>), David Bioinformatics Database (<http://david.abcc.ncifcrf.gov/summary.jsp>), and GeneSifter (<http://www.genesisifter.net/web/>) for functional annotation of hits using gene ontology, a controlled vocabulary of gene descriptors. Annotations were derived from these databases in June 2007 and restricted to those supported by experimental evidence.

Note: Supplementary Information is available on the Nature Cell Biology website.

ACKNOWLEDGEMENTS

We wish to thank Stewart Rudnicki and Caroline Shamu (Institute for Chemical and Cell Biology) for screening assistance; Jim Horn (Department of Cell Biology) for manufacturing the wound healing pin; William Pearson for conceptualizing and generating the interactive website hosted by the Cell Migration Consortium; Sabina Winograd-Katz and Benjamin Geiger (Weizmann Institute) for collaborative creation of the MAR custom siRNA library; Rick Horwitz, Alan Hall, Gaudenz Danuser and Ghassan Mouneimne for stimulating and helpful discussions and critical reading of the manuscript and Lara Petrak (Nikon Imaging Centre) for assistance with time-lapse microscopy. We are also grateful to William Hahn, David Root and The RNAi Consortium for providing shRNA vectors. Funding was from the DOD W81XWH-04-1-0360 (K.J.S.) and the Cell Migration Consortium, supported by a grant from the NIH/NIGMS GM064346 (J.S.B.). A.R., D.L. and A.K. are employees of Thermo Fisher Scientific, which supported this work in part by supplying a subset of the siRNA reagents.

AUTHOR CONTRIBUTIONS

K.J.S. designed, performed and analysed experiments and wrote the manuscript; L.M.S. created and managed the screening database and performed the informatics analysis; J.B. performed experiments; A.R. performed the knockdown quantification under the supervision of D.L. and A.K.; J.S.B. analysed and discussed data and wrote the manuscript.

COMPETING FINANCIAL INTERESTS

The authors declare no competing financial interests.

Published online at <http://www.nature.com/naturecellbiology/>

Reprints and permissions information is available online at <http://npg.nature.com/reprintsandpermissions/>

- Cram, E. J., Shang, H. & Schwarzbauer, J. E. A systematic RNA interference screen reveals a cell migration gene network in *C. elegans*. *J. Cell Sci.* **119**, 4811–4818 (2006).
- Wang, X. *et al.* Analysis of cell migration using whole-genome expression profiling of migratory cells in the *Drosophila* ovary. *Dev. Cell* **10**, 483–495 (2006).
- MacKeigan, J. P., Murphy, L. O. & Blenis, J. Sensitized RNAi screen of human kinases and phosphatases identifies new regulators of apoptosis and chemoresistance. *Nature Cell Biol.* **7**, 591–600 (2005).
- Michl, P. *et al.* CUTL1 is a target of TGF- β signaling that enhances cancer cell motility and invasiveness. *Cancer Cell* **7**, 521–532 (2005).
- Collins, C. S. *et al.* A small interfering RNA screen for modulators of tumor cell motility identifies MAP4K4 as a promigratory kinase. *Proc. Natl Acad. Sci. USA* **103**, 3775–3780 (2006).

- Zhao, Y. & Ding, S. A high-throughput siRNA library screen identifies osteogenic suppressors in human mesenchymal stem cells. *Proc. Natl Acad. Sci. USA* **104**, 9673–9678 (2007).
- Liang, C. C., Park, A. Y. & Guan, J. L. In vitro scratch assay: a convenient and inexpensive method for analysis of cell migration in vitro. *Nature Protoc.* **2**, 329–333 (2007).
- Simpson, K. J., Dugan, A. S. & Mercurio, A. M. Functional analysis of the contribution of RhoA and RhoC GTPases to invasive breast carcinoma. *Cancer Res.* **64**, 8694–8701 (2004).
- Chan, A. Y. *et al.* Roles of the Rac1 and Rac3 GTPases in human tumor cell invasion. *Oncogene* **24**, 7821–7829 (2005).
- Huang, F., Khorrova, A., Marshall, W. & Sorkin, A. Analysis of clathrin-mediated endocytosis of epidermal growth factor receptor by RNA interference. *J. Biol. Chem.* **279**, 16657–16661 (2004).
- Echeverri, C. J. & Perrimon, N. High-throughput RNAi screening in cultured cells: a user's guide. *Nature Rev. Genet.* **7**, 373–384 (2006).
- Fedorov, Y. *et al.* Off-target effects by siRNA can induce toxic phenotype. *RNA* **12**, 1188–1196 (2006).
- Jackson, A. L. *et al.* Position-specific chemical modification of siRNAs reduces "off-target" transcript silencing. *RNA* **12**, 1197–1205 (2006).
- Brembeck, F. H., Rosario, M. & Birchmeier, W. Balancing cell adhesion and Wnt signaling, the key role of beta-catenin. *Curr. Opin. Genet. Dev.* **16**, 51–59 (2006).
- Charest, P. G. & Firtel, R. A. Big roles for small GTPases in the control of directed cell movement. *Biochem. J.* **401**, 377–390 (2007).
- Gupton, S. L. *et al.* Cell migration without a lamellipodium: translation of actin dynamics into cell movement mediated by tropomyosin. *J. Cell Biol.* **168**, 619–631 (2005).
- Hugo, H. *et al.* Epithelial — mesenchymal and mesenchymal — epithelial transitions in carcinoma progression. *J. Cell Physiol.* **213**, 374–383 (2007).
- Marmor, M. D., Skaria, K. B. & Yarden, Y. Signal transduction and oncogenesis by ErbB/HER receptors. *Int. J. Radiat. Oncol. Biol. Phys.* **58**, 903–913 (2004).
- Muthuswamy, S. K., Li, D., Lelievre, S., Bissell, M. J. & Brugge, J. S. ErbB2, but not ErbB1, reinitiates proliferation and induces luminal repopulation in epithelial acini. *Nature Cell Biol.* **3**, 785–792 (2001).
- Whitehurst, A. W. *et al.* Synthetic lethal screen identification of chemosensitizer loci in cancer cells. *Nature* **446**, 815–819 (2007).
- Chen, X. & Gumbiner, B. M. Crosstalk between different adhesion molecules. *Curr. Opin. Cell Biol.* **18**, 572–578 (2006).
- Vicente-Manzanares, M., Zareno, J., Whitmore, L., Choi, C. K. & Horwitz, A. F. Regulation of protrusion, adhesion dynamics, and polarity by myosins IIA and IIB in migrating cells. *J. Cell Biol.* **176**, 573–580 (2007).
- Omelchenko, T., Vasiliev, J. M., Gelfand, I. M., Feder, H. H. & Bonder, E. M. Rhod-dependent formation of epithelial "leader" cells during wound healing. *Proc. Natl Acad. Sci. USA* **100**, 10788–10793 (2003).
- Rupp, P. A. & Kulesa, P. M. A role for RhoA in the two-phase migratory pattern of post-otic neural crest cells. *Dev. Biol.* **311**, 159–171 (2007).
- Haga, H., Irahara, C., Kobayashi, R., Nakagaki, T. & Kawabata, K. Collective movement of epithelial cells on a collagen gel substrate. *Biophys. J.* **88**, 2250–2256 (2005).
- Poujade, M. *et al.* Collective migration of an epithelial monolayer in response to a model wound. *Proc. Natl Acad. Sci. USA* **104**, 15988–15993 (2007).
- Lee, J. S., Chang, M. I., Tseng, Y. & Wirtz, D. Cdc42 mediates nucleus movement and MTOC polarization in Swiss 3T3 fibroblasts under mechanical shear stress. *Mol. Biol. Cell* **16**, 871–880 (2005).
- Lee, J. S. *et al.* Nuclear lamin A/C deficiency induces defects in cell mechanics, polarization, and migration. *Biophys. J.* **93**, 2542–2552 (2007).
- Fuja, T. J., Lin, F., Osann, K. E. & Bryant, P. J. Somatic mutations and altered expression of the candidate tumor suppressors CSNK1 epsilon, DLG1, and EDD/hHYD in mammary ductal carcinoma. *Cancer Res.* **64**, 942–951 (2004).
- Debnath, J., Muthuswamy, S. K. & Brugge, J. S. Morphogenesis and oncogenesis of MCF-10A mammary epithelial acini grown in three-dimensional basement membrane cultures. *Methods* **30**, 256–268 (2003).
- O'Brien, J., Wilson, I., Orton, T. & Pognan, F. Investigation of the Alamar Blue (resazurin) fluorescent dye for the assessment of mammalian cell cytotoxicity. *Eur. J. Biochem.* **267**, 5421–5426 (2000).
- Root, D. E., Hacohen, N., Hahn, W. C., Lander, E. S. & Sabatini, D. M. Genome-scale loss-of-function screening with a lentiviral RNAi library. *Nature Methods* **3**, 715–719 (2006).
- Irie, H. Y. *et al.* Distinct roles of Akt1 and Akt2 in regulating cell migration and epithelial-mesenchymal transition. *J. Cell Biol.* **171**, 1023–1034 (2005).
- Zaidel-Bar, R., Itzkovitz, S., Ma'ayan, A., Iyengar, R. & Geiger, B. Functional atlas of the integrin adhesome. *Nature Cell Biol.* **9**, 858–867 (2007).

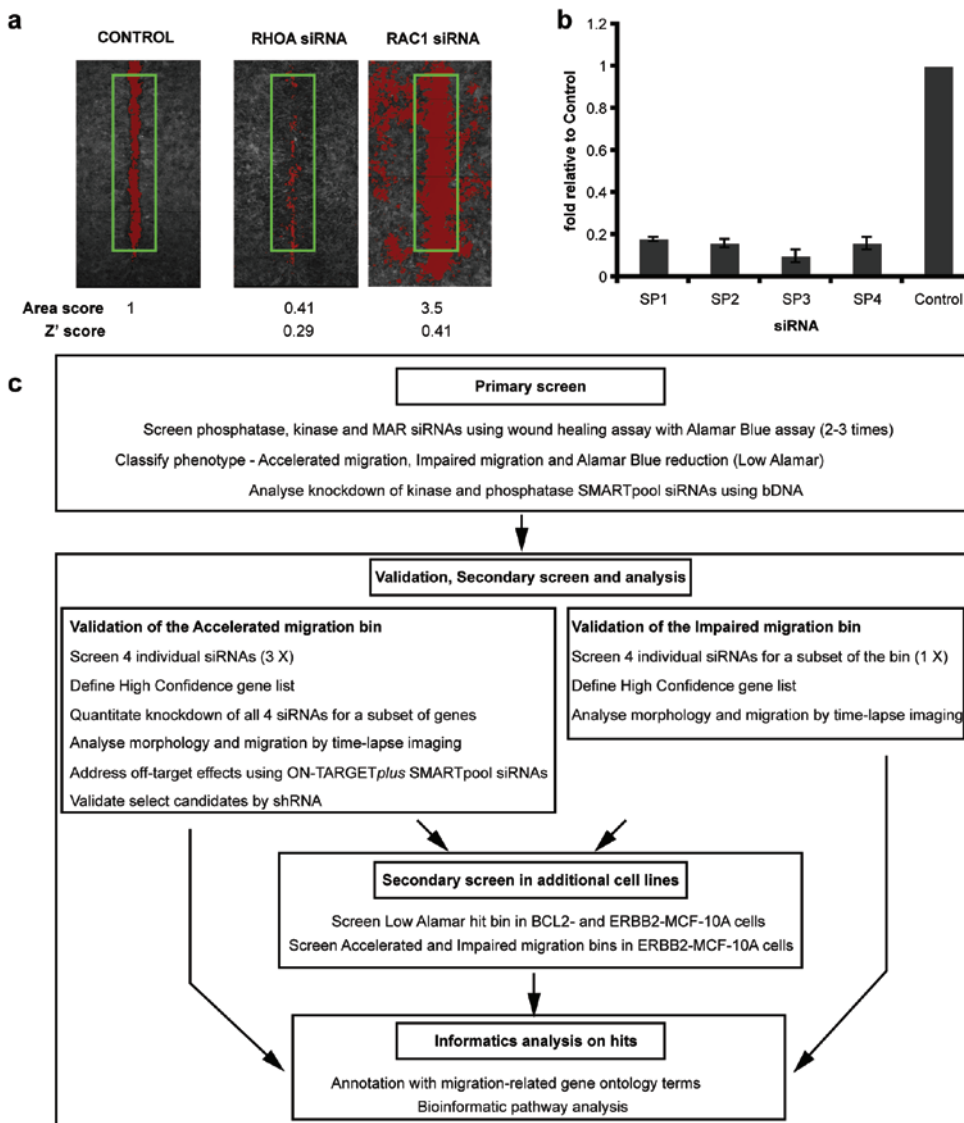


Figure S1 Validation and schematic workflow of the wound healing screen. A) Wound healing assay reproducibility. To quantitate migration, the cells were fixed and labelled with rhodamine-conjugated phalloidin and imaged by automated fluorescent microscopy. Motility, termed the 'area score' was quantitated by measurement of the cleared area (shown in red) in a uniformly marked region (demarcated by the green box) using MetaExpress threshold analysis. After normalisation, the mock transfection control was set at 1. Knockdown of *RHOA* accelerates motility with an area score of 0.41. Knockdown of *RAC1* impedes migration, resulting in an open wound area and score of 3.5. The Z' factor, a statistical measurement of the robustness and reproducibility of the motility scores were 0.29 and 0.41 respectively.

SMARTpool reproducibility was 88% between duplicate plates from the same day and 83.7% of SMARTpools showed the same phenotype across all experiments. B) Knockdown of PP1B was >80% relative to the mock-transfected control for each of four different SMARTpools (SP1-4), analysed on three independent days in triplicate. Shown as the average +/- SD. C) Hits were classified based on the SMARTpool screens, which were subsequently validated by screening with individual siRNA sequences. Each siRNA was assayed in duplicate with multiple biological replicates. Concentrating on the Accelerated and Impaired hit bins, higher resolution analysis of the cellular morphology and time-lapse imaging were performed. All hits were analysed for migration and adhesion associated Gene Ontology terms and pathway linkages.

SUPPLEMENTARY INFORMATION

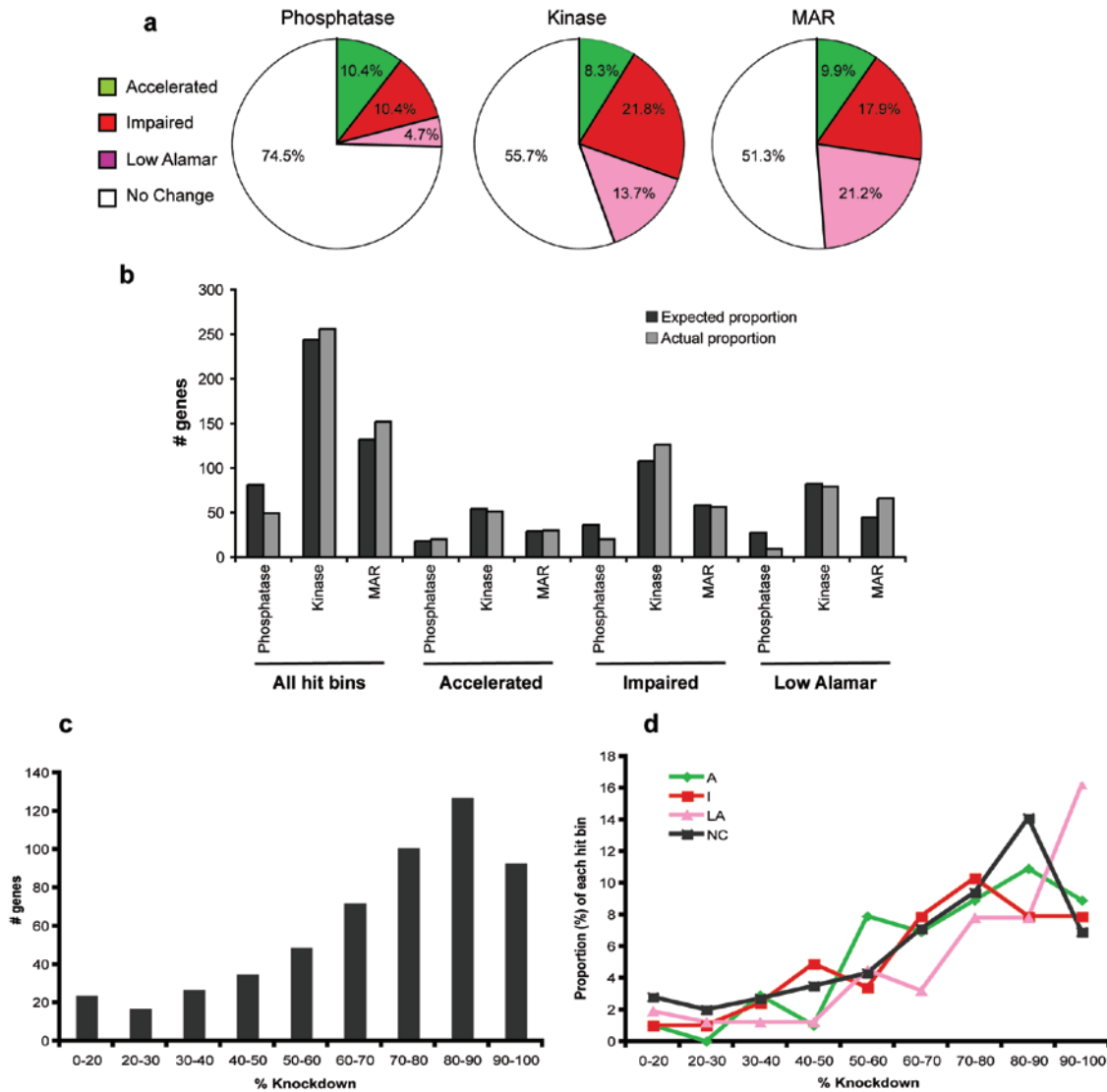


Figure S2 Distribution of the phenotypic hit bins, proportional representation of the hits within each bin and quantitation of knockdown. A) The relative proportions of the Accelerated (green), Impaired (red), Low Alamar (pink) and No Change (white) bins for each library. B) Breakdown of the proportion of SMARTpools in the phosphatase, kinase and MAR libraries (expected) compared to the actual proportion observed. 'All hit bins' represent the merge of the Accelerated, Impaired and Low Alamar bins and is compared with the breakdown for each individual bin. These data show the phosphatases were under-represented as a group ($p=9.28 \times 10^{-6}$) when comparing all hits and that the Low Alamar bin contributed significantly to the under-representation. Similarly the kinases were over-represented in the Impaired bin. C) Of the 762 genes analysed for knockdown (kinases

and phosphatases), 42% of siRNAs targeted greater than 70%. 28% of the library (217 genes) was not analysed due to technical reasons. The extent of knockdown for each gene is indicated online, www.cellmigration.org. A high proportion (43.7%) of the phosphatase genes were not detectable in the bDNA assay. One possible explanation for the proportionately higher number of No Change phenotypes in the phosphatase library may be that a number of genes are very poorly, or not expressed in the MCF-10A cell line. D) Separating the contribution of each phenotypic hit bin relative to knockdown shows there was no significant enrichment for knockdown in any category ($p>0.05$, ANOVA, Kolmogorov-Smirnov test). Presented as a proportion of the total number of genes in each bin. A=Accelerated, I=Impaired, LA=Low Alamar, NC=No change.

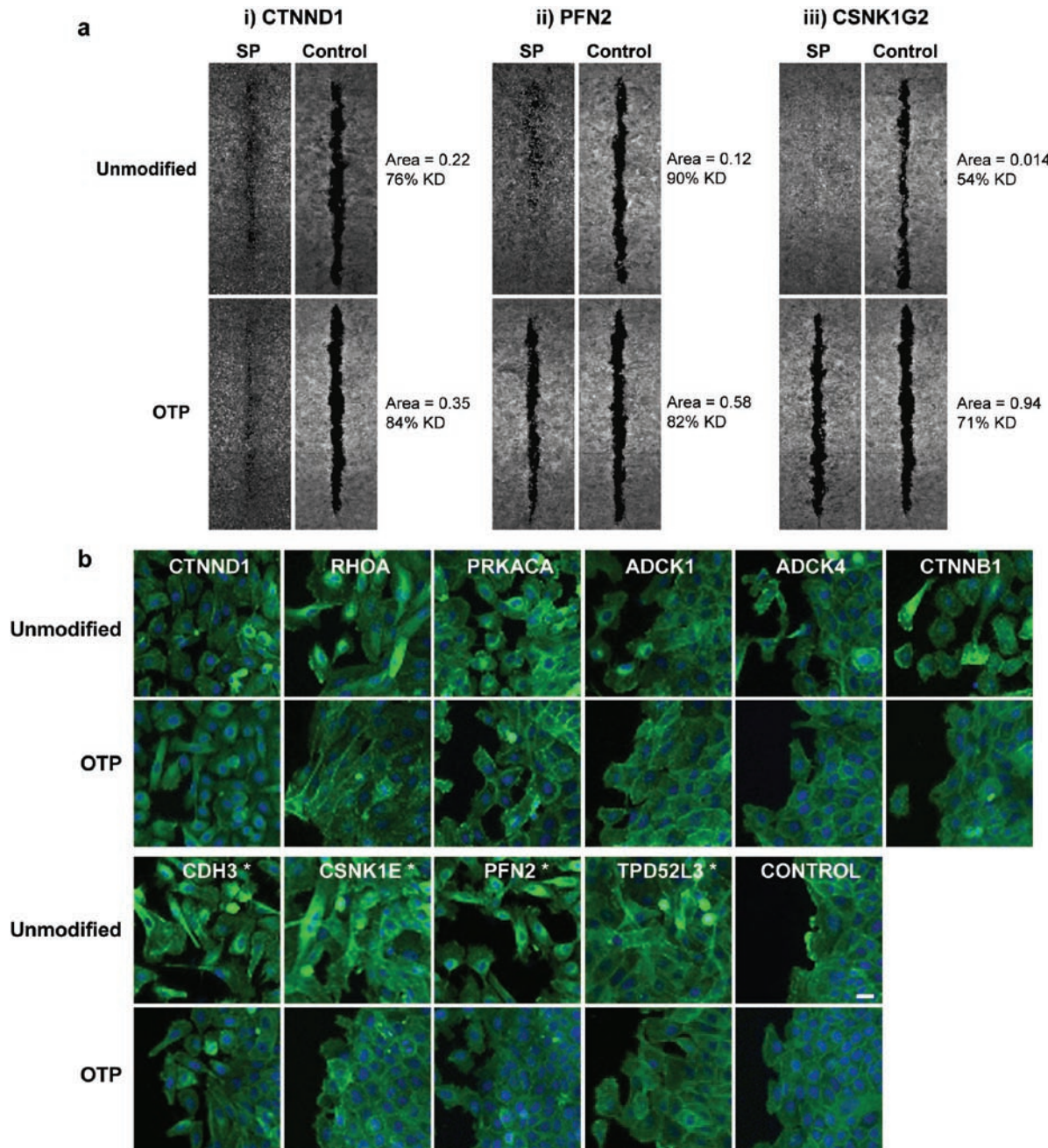


Figure S3 Comparison of the wound healing phenotype for unmodified- and ON-TARGETplus-modified (OTP) SMARTpools. Robust migration and morphology was observed for *CTNND1*, *PRKACA*, *RHOA*, *ADCK1*, *ADCK4* and *CTNNB1*, while *CDH3*, *CSNK1E*, *PFN2* and *TPD52L3* showed much weaker phenotypes. A) Comparison of wound closure, area score and extent of knockdown (KD) for the following SMARTpool siRNA reagents (SP) i) *CTNND1* showed a consistent phenotype using both reagents, ii) *PFN2*, both reagents generated an Accelerated migration phenotype but the OTP reagent was much weaker and iii) *CSNK1G2*, the OTP reagent generated an

area score outside the cut-off range but was visually over-ridden as a very weak Accelerated phenotype. The phalloidin channel wounding montage is shown in gray scale. B) Similar morphological changes were observed for those genes that showed a robust Accelerated migration phenotype with the OTP reagent. The OTP siRNAs that generated a weaker wound healing phenotype typically showed less morphological distinction compared with the unmodified SMARTpools. Those that had a much weaker migration phenotype but were still considered to accelerate wound closure are indicated by *. The scale bar represents 25 μ M.

SUPPLEMENTARY INFORMATION

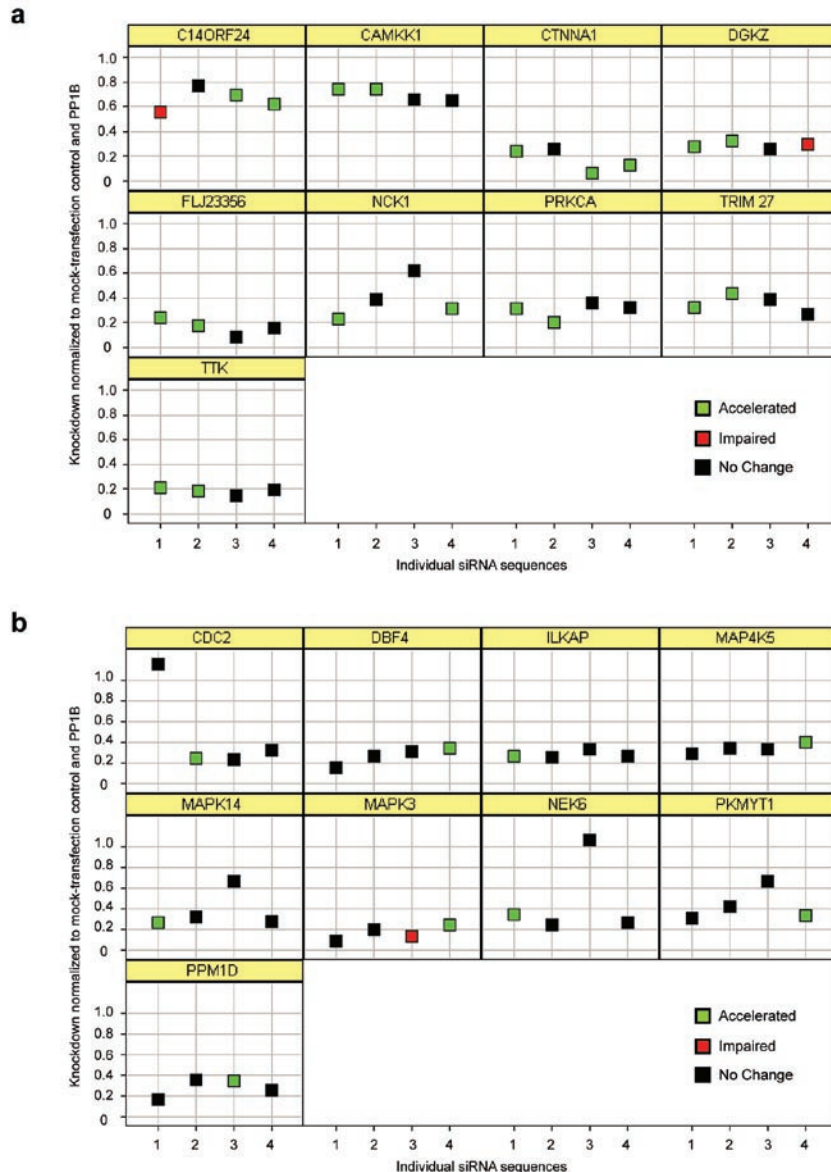


Figure S4 Quantitation and correlation with phenotype of the extent of knockdown for the MC and Discordant individual Accelerated migration siRNAs. Knockdown was quantitated using bDNA in parallel with wound healing for all four individual siRNA sequences. The

trellised box plots show the extent of knockdown for each siRNA and the wound healing phenotype, indicated in green for Accelerated, black for No Change and red for Impaired. A) MC siRNAs. B) Discordant siRNAs.

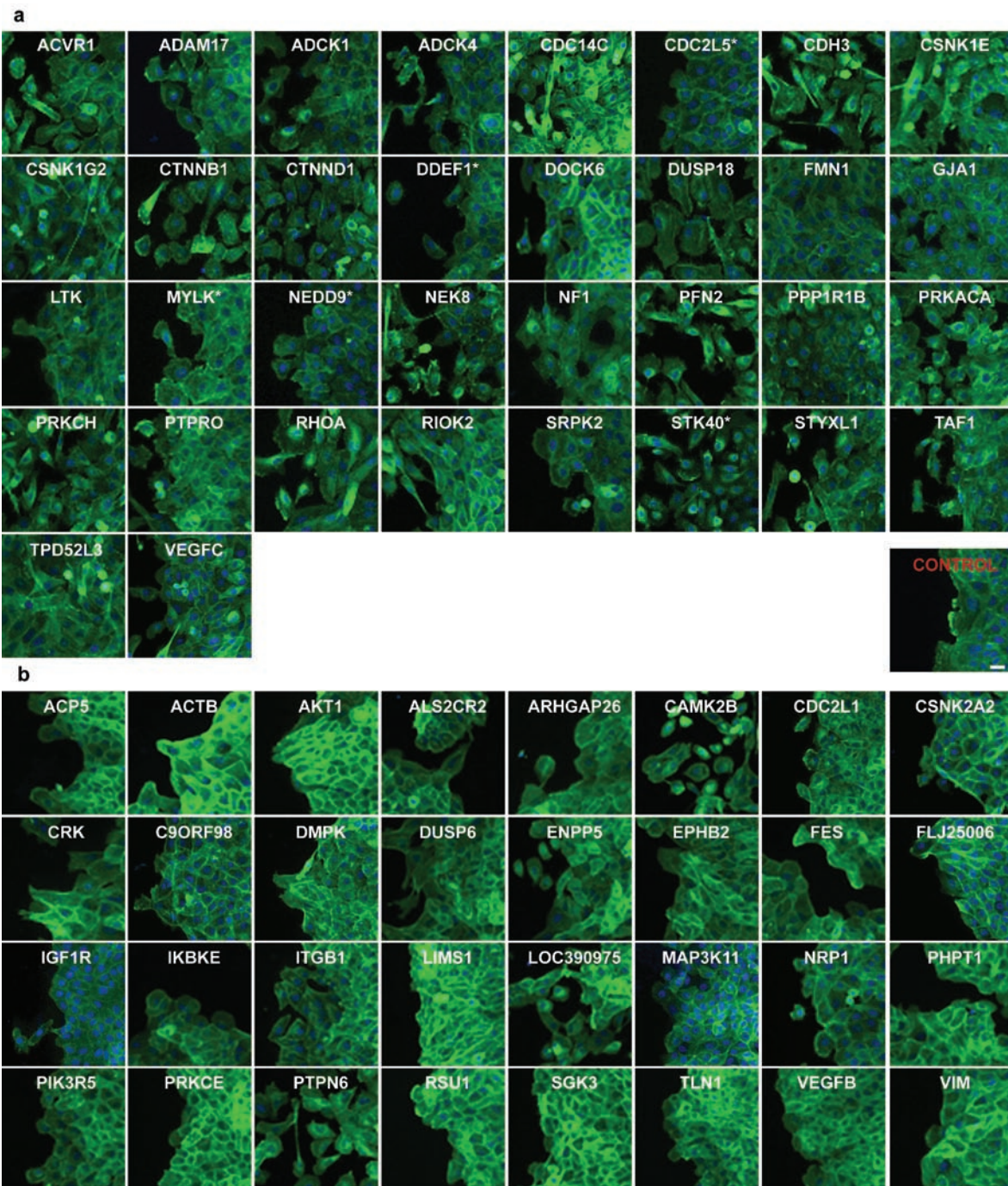


Figure S5 Comparison of the cellular morphologies at the wound edge for all the HC Accelerated and Impaired migration hits. A) Accelerated, B) Impaired. Representative images are shown (phalloidin (green) and DAPI

(blue)). Cells migrated from right to left. Genes that were considered HC on the basis of ON-TARGET*plus* validation are indicated by *. The scale bar represents 25 μ M.

SUPPLEMENTARY INFORMATION

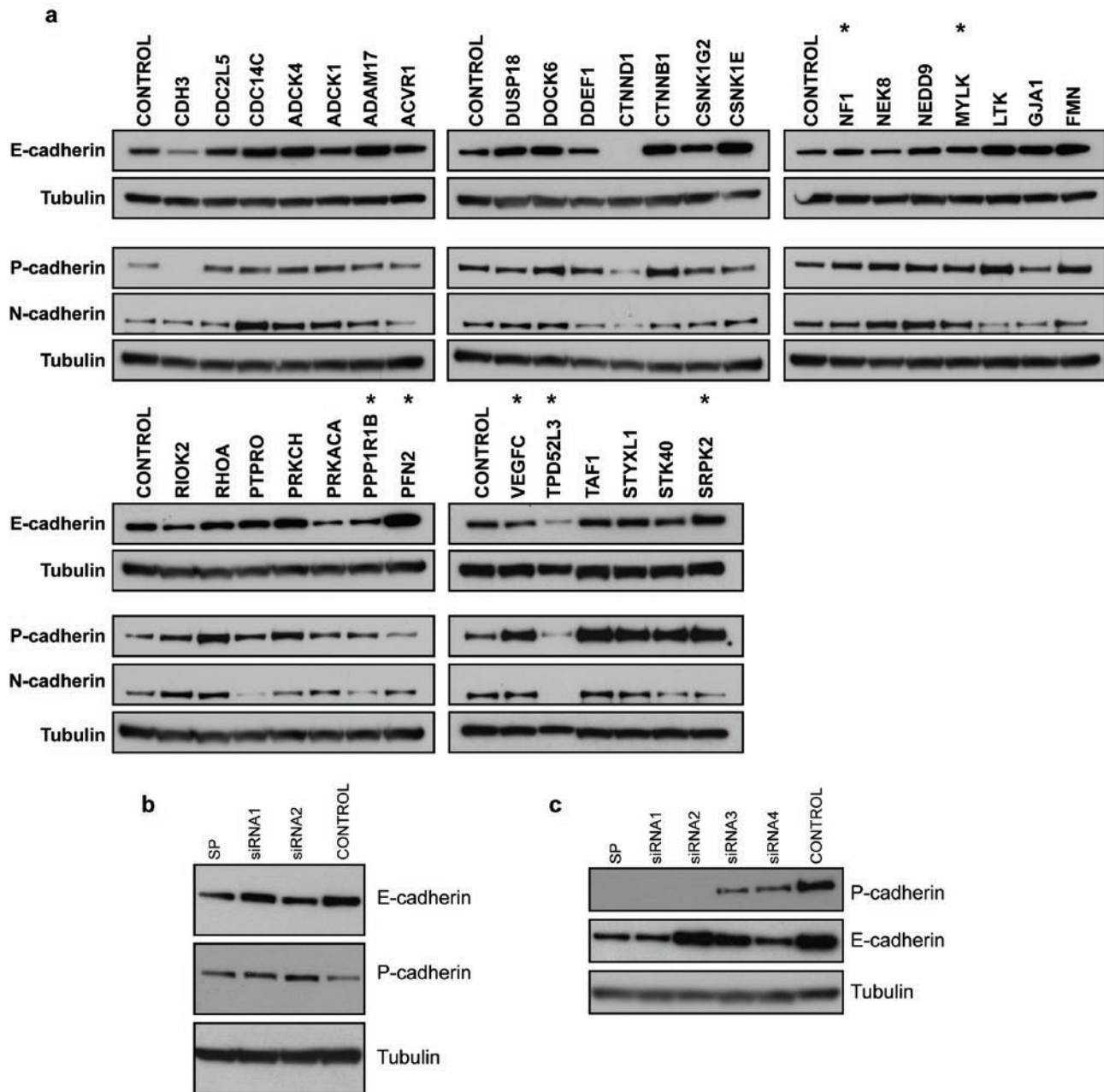


Figure S6 Expression profiles of adhesion proteins for the HC Accelerated migration siRNAs. A) Analysis of SMARTpool knockdown at the protein level was performed 48 hours post transfection. All siRNAs were transfected simultaneously. The expression levels of E-cadherin, P-cadherin and N-cadherin are shown relative to tubulin. Genes indicated by * were not

reproducible upon repeating with a second series of lysates. B) Knockdown of *CDH1* (E-cadherin) SMARTpool and two individual siRNAs shows the protein was inefficiently targeted. C) Knockdown of *CDH3* (P-cadherin) SMARTpool and four individual siRNAs shows a dramatic reduction in expression levels and down-regulation of E-cadherin.

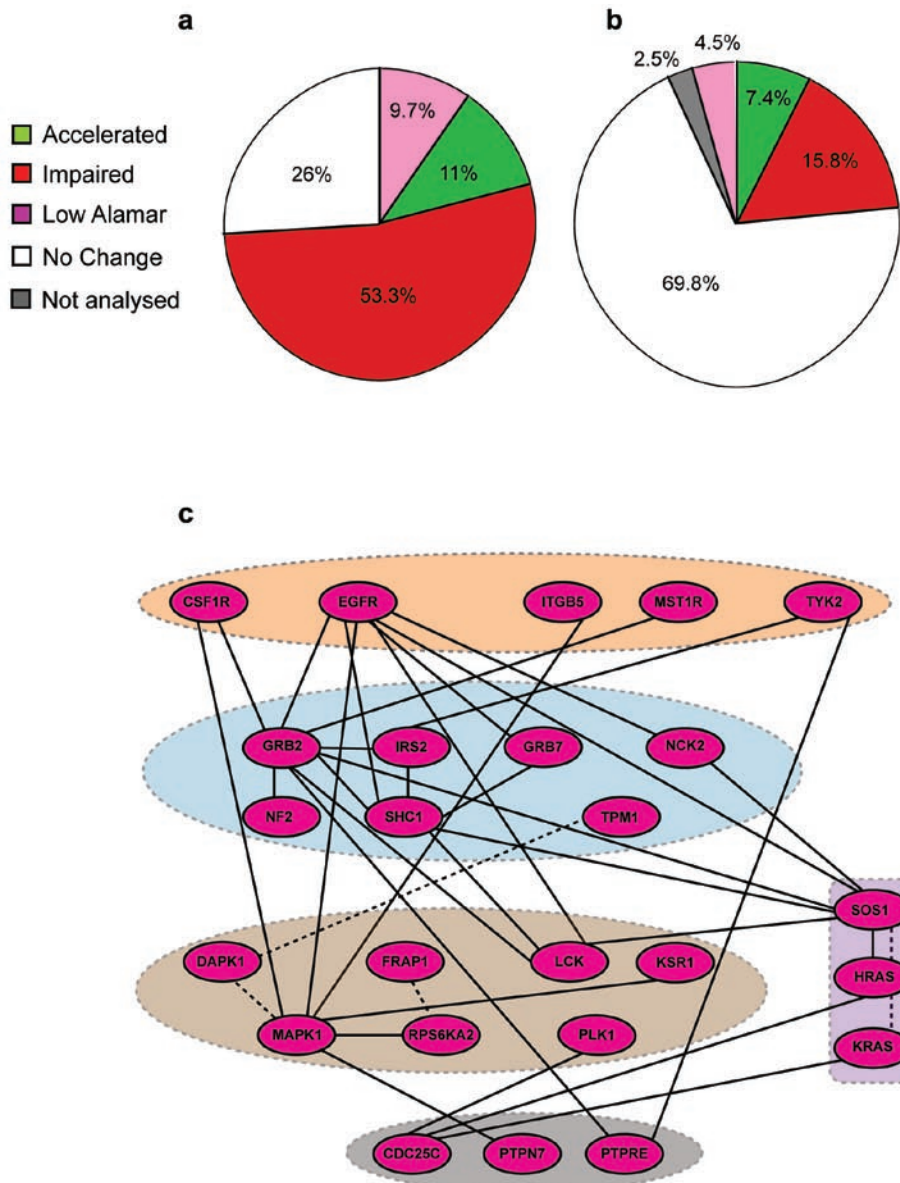


Figure S7 Summary of the phenotypes observed after screening the Low Alamar and Impaired migration bins in the ERBB2-MCF-10A cells and the Low Alamar signalling network. A) Low Alamar screen and B) Impaired screen. C) Direct relationships were integrated for the MC Low Alamar siRNAs and those siRNAs that also scored as Low Alamar hits in the ERBB2 background. The proteins in this network include multiple components

of the EGFR/receptor tyrosine kinase signalling pathway. The genes have been classified into GTPase/GTPase regulators (shaded purple), receptors (orange), adaptors (light blue), kinases (brown) and phosphatases (grey). Solid lines indicate direct interactions established by Ingenuity and dashed lines represent interactions determined from the following protein-protein interaction databases (BioGrid, HPRD).

SUPPLEMENTARY INFORMATION

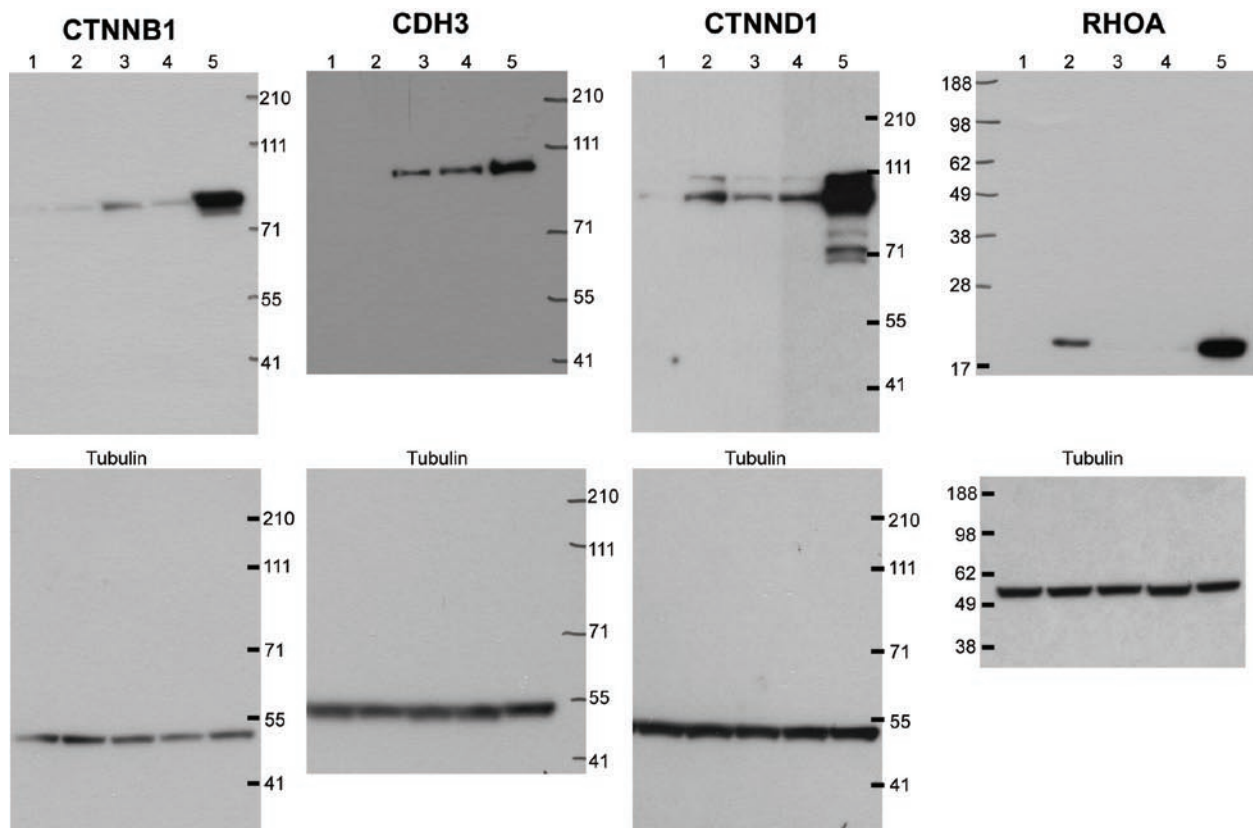


Figure S8 Full scans of the immunoblots shown in Figure 2b

Supplementary Discussion

Results

Validation of selected genes using an shRNA approach

Eleven genes that accelerated migration were randomly chosen for further validation by stable knockdown using lentiviral vectors encoding shRNAs. We evaluated four or five shRNAs for each gene under standard assay conditions and detected accelerated migration for one or more shRNAs targeting *ADCK4* (HC), *CTNNB1* (HC), *CTNND1* (HC), *ENPP1* (Discordant), *GJA1* (HC), *MAPK14* (Discordant), *NCK1* (MC), *NEK8* (HC), *PPM1D* (Discordant), *PTPRO* (HC) and *RHOA* (HC). The remaining sequences showed No Change. From these analyses we gained more confidence that some of the Discordant genes could be reassigned with further analysis. While we have not validated mRNA or protein knockdown for all of these hairpins, identifying similar phenotypes using alternative reagents provides further validation for the screen and the specific genes analysed. Stable knockdown vectors encoding shRNAs will be very useful for mechanistic studies requiring longer-term assays.

Discussion

Using Gene Ontology (GO) annotation, 212 of the 1081 genes screened (19.6%) have been previously linked to cell migration or adhesion in any cell type or assay using traditional hypothesis-driven, non-high-throughput methods. We identified 46 of these genes as High or Moderate confidence regulators of migration (Table 1; Supplementary Table 2A, B, C). Only the Accelerated and Impaired HC bins were enriched in known migration or adhesion genes; 2.2-fold in the Accelerated set ($p=0.029$) and 2.8-fold in the Impaired set ($p=0.012$).

Forty-two HC genes (22 Accelerated and 20 Impaired) have no prior association with cell migration or adhesion using these GO terms as specific criteria (Table 1). Twelve of these have no experimentally supported GO annotation (*ADCK1*, *ADCK4*, *CDC14C*, *CDC2L5*, *CSNK2A2*, *C9orf98*, *DOCK6*, *ENPP5*, *FLJ25006*, *LOC390975*, *NEK8*, *RIOK2*), while the remaining 30 have been characterised to various extents, with 17 involved in major cellular processes, including ‘cell death’, ‘cell proliferation’, ‘cell cycle’ and ‘cell differentiation’. Many of these are likely to be involved in central pathways that can impinge on multiple processes including cell migration.

To further investigate the three major signalling nodes, β -catenin, $\beta 1$ -integrin and actin, each node was entered separately into the Ingenuity Network Explorer and all direct, up- and down-stream interactors were identified. These gene lists were then cross-referenced against the HC gene list; then, to gain more pathway information we included the MC Accelerated and Impaired genes and those that reverted the Low Alamar or Impaired phenotypes in the ERBB2 background. We interrogated several protein interaction databases (Bind, BioGrid, HPRD, Ingenuity and the Adhesome¹) and identified extended network linkages (Figure 7A, B and C) that are discussed in detail below.

The β -catenin network.

β -catenin (*CTNNB1*) regulates cell adhesion through its interaction with classic cadherins and other junctional proteins, but also mediates pleiotrophic changes in cell behaviour through its activity as a nuclear transcriptional regulator². siRNAs targeting most of the HC hit genes that directly interact with β -catenin (*CDH3*, *CSNK1E*, *GJA1*, *CTNNB1*, *CTNND1*) accelerated migration and caused dissociation of cells from the epithelial sheet, supporting a role for these genes in regulating cell-cell adhesion in MCF-10A cells (Figure 7A). Interestingly, HC Impaired genes *PTPN6* and *CSNK2A2* also interact directly with β -catenin and showed altered cell-cell adhesion and erratic migratory behaviour

despite impairing migration. Of the Accelerated Group D siRNAs that showed weak cell-cell adhesion by time-lapse imaging, only PTPRO has been linked to β -catenin signalling. This phenotype is consistent with the ability of PTPRO to reverse EGF- and v-src induced tyrosine phosphorylation of β -catenin and suppress migration of human pancreatic adenocarcinoma cells³. By static imaging, α -catenin (CTNNA1; MC Accelerated) showed some loss of cell-cell adhesion primarily at the wound edge.

Cadherin family receptors are the major cellular mediators of cell-cell adhesion. Of the classic cadherins, MCF-10A cells express E-cadherin and P-cadherin and variable levels of N-cadherin, depending on cell density. P-cadherin is typically associated with basal cells of epidermal derived tissues⁴ and MCF-10A cells display an expression signature typical of basal cells⁵. It is noteworthy that the only cadherin family gene implicated in migration in this screen was CDH3 (P-cadherin); down-regulation of E-cadherin scored as No Phenotype and N-cadherin as Discordant (from original Impaired bin). Knockdown of E-cadherin mRNA was not analysed, but the SMARTpool and two individual sequences did not target effectively (Supplementary Information, Fig. S6B). Down-regulation of P-cadherin protein and mRNA was very efficient (Figure 2) and was associated with a striking disruption of cell adhesion and acceleration of migration; interestingly, the P-cadherin SMARTpool siRNA reagent decreased expression of E-cadherin (Supplementary Information, Fig. S6A, C). These results provide explanations for the dramatic disruption of cell-cell adhesion by P-cadherin knockdown and the lack of effect of E-cadherin siRNAs.

CSNK1E has been shown to regulate β -catenin (Figure 7A)⁶ and to inhibit cell-cell adhesion through phosphorylation of the cytoplasmic domain of E-cadherin⁷. Knockdown of *CSNK1E* and *CSNK1G2* resulted in a HC Accelerated migration phenotype coupled with minimal cell-cell adhesion and rapid and erratic migration. SMARTpool siRNA reagents targeting six of the seven other casein kinase family members Impaired migration, with *CSNK2A2* validating with HC and interacting directly with β -catenin. Both *CSNK1D* and *CSNK1G1* scored Impaired when screened in ERBB2 cells and on this basis, *CSNK1D* is also implicated in β -catenin signalling (Figure 7A). Dichotomous roles for casein kinase 1 isoforms have been previously described, e.g. in the canonical Wnt pathway, where *CSNK1A* is a negative regulator, whereas *CSNK1G3*, *CSNK1D* and *CSNK1E* positively regulate this pathway⁸.

Connexin 43 (GJA1), a down-stream effector of β -catenin⁹ is an intercellular junction protein and tumour suppressor gene, that is often down-regulated in breast cancer. Over-expression dramatically reduces the invasiveness of some tumour cell lines¹⁰ and down-regulation at wound sites has been shown to enhance migration, supporting the relevance of our findings¹¹. Video microscopy revealed that reduced expression significantly impairs cell-cell contact and causes erratic migration. Large, broad protrusions and long retraction tails suggest abrogation of myosin signalling. Further studies are required to identify the mechanism of adhesion disruption. PTPN6 is also involved in $\beta 1$ -integrin signalling, and while predominant in hematopoietic cells, it appears to play multiple roles in various human epithelial cancers¹². Consistent with its importance in cell-cell and cell-substratum adhesion, loss of this gene resulted in loss of cell-cell contact within the monolayer and an almost complete inability to migrate. It is possible that lack of substratum adhesion impedes the ability of the cells at the leading edge of the wound to make adhesive contacts sufficient for motility.

PKD2, a downstream target of β -catenin has been shown to regulate branching morphogenesis of the developing kidney¹³ and associates with NEK8, a HC Accelerated gene, that has been shown to regulate cell-cell adhesion in association with PKD2¹⁴. Consistent with this data, knockdown of NEK8 causes a significant reduction in cell-cell contact.

The strong correlation between MCF-10A cell motility and weak cell-cell adhesion is not surprising^{15, 16}, however, this is the first systematic study that demonstrates a strong correlation between weakened adhesion and enhanced motility. The time-lapse video microscopy data suggests the enhanced migration is at least in part a consequence of release of constraints imposed by cell-cell junctional interactions in the epithelial sheet; however, the alterations in adherens junctions could affect motility more directly by altering the localisation, interactions and dosage of signalling and cytoskeletal proteins that affect cell motility. Alternatively, the loss of adhesion could be a secondary consequence of cytoskeletal alterations more directly responsible for enhanced motility. Interestingly, the majority of the genes that accelerated migration and caused some degree of cell dissociation have not been implicated in cell-cell adhesion and weren't linked in the network with known junctional proteins (*ADCK4*, *CDC14C*, *CSNK1G2*, *DDEF1*, *DOCK6*, *PFN2*, *PPP1R1B*, *PRKCH*, *STK40*, *STXYL1*, *TPD52L3*). Of these genes only *DDEF1* has been implicated in the regulation of cell migration¹⁷.

The β 1-integrin network.

To fully interrogate the β 1-integrin network, we created a Focal Adhesion gene set by combining the Adhesome protein database¹, Focal Adhesion GO and literature annotation (Figure 7B; Table S5) and found that the HC Impaired genes contributed significantly to this network ($p=0.001$). This network has been drawn to highlight the major interacting groups, including GTPases and GTPase regulators, adaptors, actin regulators and a number of kinases and phosphatases.

From the Focal Adhesion gene set, seven of nine genes from the Impaired bin and four of five genes from the Accelerated bin have been implicated in migration. ARHGAP26 (GRAF), PTPN6 and PTPRO have not been strictly linked to migration. ARHGAP26 is a GTPase activating protein for RHOA that associates with Focal Adhesion Kinase (FAK)¹⁸ and when over-expressed decreased Rho-activation and suppressed stressed fibers¹⁹, suggesting that it could be involved in dynamic aspects of focal adhesion formation critical for cell migration. PTPRO has previously been linked to axon outgrowth and negatively regulates ephrin receptors, which regulate migration in multiple cell types. Down-regulation of one Ephrin family member, EPHB2²⁰, also impaired migration with HC.

Multiple focal adhesion-associated proteins scored with MC as well: the Accelerated bin includes ENAH (MENA), NCK1, PARVA (Parvin), PRKCA (PKC α), SLK and N-WASP (WASL); the Impaired bin includes PARVG (Parvin), RAC1 and TNS1 (tensin). Many other focal adhesion proteins that inhibited migration induced a Low Alamar phenotype (BCAR3, GRB7, NCK2, PXN (paxillin), SVIL and TLN2; Supplementary Information, Table S5). All except TLN2 were rescued and impaired migration when re-screened in the ERBB2 background, thus implicating them in migration as well. The majority of these genes are linked in the β 1-integrin pathway (Figure 7B).

The finding that many integrin-linked and focal adhesion proteins affect cell migration is not surprising given the important role of matrix adhesion in this process and the identification of these genes in this screen provide further validation of the screen. MCF-10A cells express multiple integrins and secrete several matrix proteins (e.g. collagens and laminins) that serve as ligands for β 1 integrins. A large number of the integrin family members were screened, yet knockdown of only β 1 caused a dramatic phenotype. siRNAs targeting integrins α 6 and β 4, receptors for laminin, showed no effect. This may reflect the dominance of β 1 in adhesive interactions critical to migration in a wound healing format or the possible failure of other integrin siRNAs to knockdown effectively.

The Actin network.

Enrichment of actin interactive proteins in the HC data set was expected given their critical role in regulation of the cytoskeleton and cell motility. We observed a similar number of HC Impaired and Accelerated genes that interact directly with Actin (Figure 7C). It is interesting that *PFN2* siRNAs accelerated migration since the related isoform *PFN1* impaired migration and both play a critical role in actin polymerisation through catalysis of ATP exchange on actin monomers, promoting their addition to filament barbed ends. Nine of the 12 genes identified in the network after screening in the ERBB2 background impaired migration (*ARPC1B*, *ARHGEF18*, *CDH2*, *FLNA*, *NCAM1*, *PFN1*, *RDX*, *SHC1*, *ZBP1*).

Fourteen myosin or myosin-regulatory proteins were screened, and perhaps surprisingly, only two scored a phenotype; the myosin regulatory kinase, *MYLK* scored HC Accelerated and *MYL5* scored MC Low Alamar which was rescued by ERBB2 expression. Of the actin nucleator ARP family members, *ARPC2* and *ARPC5* both scored MC Impaired and had no phenotype in ERBB2 cells, *ARPC1B* scored MC Low Alamar which was rescued by ERBB2 and the remainder *ARPC1A*, *ARPC3*, *ARPC4* and *ACTR3* all scored Discordant phenotypes from the original No Change bin.

RHO family

Knockdown of *RHOA* accelerated migration; however, we did not observe any significant enrichment in either the HC or MC hit lists for any of the 10 other RHO GTPases family members that were assayed. The majority of exchange factors showed Discordant phenotypes that originated from the No Change bin. Knockdown of *RAC1*, required for lamellipodial dynamics in many cell types²¹ scored MC Impaired, while *CDC42*, a protein that regulates motility polarity and directionality²¹, scored a Discordant No Change, suggesting it is either not important for polarity or directionality in MCF-10A cells or these siRNAs target the gene inefficiently.

Low Alamar and EGFR signalling

Pathway analysis of the Low Alamar MC and ERBB2 bin genes revealed a strong bias around the canonical EGFR/receptor tyrosine kinase signalling pathway (Supplementary Information, Fig. S7C). While EGF activates pathways that suppress apoptosis, the failure of *BCL2* to rescue most of the Low Alamar siRNAs suggests that the Low Alamar score does not primarily reflect apoptotic cell death. Because MCF-10A cells require EGF for proliferation, the reduced Alamar Blue score could in part be due to suppression of proliferation. However, other studies in our lab have shown that withdrawal of EGF dramatically decreases Alamar Blue reduction independent of proliferative and anti-apoptotic effects (Z. Schafer and J. S. B. data not shown). This raises the possibility that EGF regulates metabolic activity in MCF-10A cells. Indeed, knockdown of EGFR in MCF-10A cells resulted in a MC Low Alamar phenotype that was rescued by ERBB2. Several Low Alamar bin genes, including *IRS2*, *RAS*, *PI3K*, *AKT1*, and *FRAP1* (mTOR) have all been implicated in regulating intracellular nutrient uptake and/or energy balance²²⁻²⁴. It is likely that the ability of ERBB2 over-expression to rescue the Low Alamar phenotype in the vast majority of cells is due to rescue of both proliferative and metabolic impairments. Given the importance of the EGFR pathway in this phenotype and the fact that our screen identified major components of this pathway, it is intriguing to speculate that further study of some of the poorly characterised Low Alamar genes may identify new genes that regulate cellular energy homeostasis.

While some of the siRNAs targeting cell adhesion proteins like *BCAR3*, *ELMO3* and *TPM1* may cause a Low Alamar score by inducing cell detachment, there was no enrichment for adhesion GO categories in the Low Alamar MC gene set, so it is either unlikely that loss of adhesion represents the major cause of the Low Alamar phenotype or that we have identified new adhesion-related genes that require further investigation.

Cancer associated implications from the screen

Cancer progression is associated with abrogation of normal controls that limit cell migration and invasion, eventually leading to metastasis, the major cause of morbidity associated with tumourigenesis. Cells must adopt new characteristics to carry out cellular processes associated with invasion and metastasis and invasiveness is typically associated with enhanced migration, alterations in adhesion proteins, and loss of cell-cell contact. Many of the siRNAs analysed in this screen induced such properties in MCF-10A cells raising the possibility that the reductions in the levels of these genes may be associated with migratory phenotypes of cancer cells. In addition, siRNAs that suppressed migration could target proteins that drive migration of tumour cells. The most obvious candidate genes that could contribute to invasion/metastasis would be those genes whose reduction by siRNA cause cell-cell dissociation, a property associated with tumour cell dissemination. The majority of the HC and MC Accelerated bin siRNAs induced cell dissociation and altered the expression or localisation of E-cadherin. Suppression or relocalisation of E-cadherin is associated with tumour initiation and progression in several epithelial cancers²⁵. For example, reduced expression and aberrant localisation of the HC Accelerated gene *CTNND1* are among the most common events associated with many epithelial tumours^{26, 27}. *CSNK1E*, a Accelerated bin gene that caused reduced cell-cell adhesion when down-regulated, is expressed at low levels in poorly differentiated, higher grade tumours and there is a positive association between loss of heterozygosity and somatic mutations in *CSNK1E* in breast tumours²⁸. *NF-1*, another Accelerated bin gene, is a well characterised tumour suppressor, acting at the level of RAS suppression²⁹. PTPRO has been implicated in tumour suppression in human lung, liver and colon cancer based on methylation studies and loss of expression observed in the majority of primary liver and lung tumours³⁰. *In vitro* over-expression studies suggest a role for PTPRO in regulating anchorage independent proliferation and survival; however, our studies suggest that loss of this phosphatase might enhance migratory activity of tumour cells. NEK8 induced cell dissociation and increased motility and while largely unstudied, a recent report suggests it is associated with breast tumourigenesis, with increased expression in tumour tissue compared with normal breast³¹.

A number of other genes identified in this screen have been implicated in cancer due to their gain of expression in tumours. From the HC Impaired bin, the best characterised gene associated with cancer is Akt which is frequently activated in tumour cells due to hyperactivation of the PI3K pathway resulting from mutations in PIK3CA, its 85 kDa regulatory subunit or loss of the PIP3 negative regulator PTEN; however, it is also amplified or mutated in some tumours³². A distinct regulatory subunit of PI3K, PIK3R5, scored as a HC Impaired bin hit; however this particular subunit has not been implicated in cancer. IKBKE, which regulates NFKB, is amplified in breast tumours³³ and other hit genes including DUSP6³⁴, RSU1 (www.oncomine.org), EPHB2³⁵, NRP1³⁶ and ARHGAP26³⁷ are frequently up-regulated in tumours. RSU1 is particularly interesting with respect to basal, high grade breast tumours where it is selectively and significantly up-regulated in this subtype of breast tumours (www.oncomine.org). Closer inspection of the role of these genes in tumour cell migration and cancer is warranted based on our studies.

References

1. Zaidel-Bar, R., Itzkovitz, S., Ma'ayan, A., Iyengar, R. & Geiger, B. Functional atlas of the integrin adhesome. *Nat. Cell. Biol.* **9**, 858-867 (2007).
2. Brembeck, F.H., Rosario, M. & Birchmeier, W. Balancing cell adhesion and Wnt signaling, the key role of beta-catenin. *Curr. Opin. Genet. Dev.* **16**, 51-59 (2006).
3. Yan, H.X. *et al.* Physical and functional interaction between receptor-like protein tyrosine phosphatase PCP-2 and beta-catenin. *Biochemistry*. **41**, 15854-15860 (2002).
4. Knudsen, K.A. & Wheelock, M.J. Cadherins and the mammary gland. *J. Cell. Biochem.* **95**, 488-496 (2005).

5. Neve, R.M. *et al.* A collection of breast cancer cell lines for the study of functionally distinct cancer subtypes. *Cancer Cell*. **10**, 515-527 (2006).
6. Gao, Z.H., Seeling, J.M., Hill, V., Yochum, A. & Virshup, D.M. Casein kinase I phosphorylates and destabilizes the beta-catenin degradation complex. *Proc. Natl. Acad. Sci. U S A*. **99**, 1182-1187 (2002).
7. Dupre-Crochet, S. *et al.* Casein kinase 1 is a novel negative regulator of E-cadherin-based cell-cell contacts. *Mol. Cell Biol.* **27**, 3804-3816 (2007).
8. Price, M.A. CKI, there's more than one: casein kinase I family members in Wnt and Hedgehog signaling. *Genes Dev.* **20**, 399-410 (2006).
9. Miller, J.R., Hocking, A.M., Brown, J.D. & Moon, R.T. Mechanism and function of signal transduction by the Wnt/beta-catenin and Wnt/Ca²⁺ pathways. *Oncogene*. **18**, 7860-7872 (1999).
10. McLachlan, E., Shao, Q., Wang, H.L., Langlois, S. & Laird, D.W. Connexins act as tumor suppressors in three-dimensional mammary cell organoids by regulating differentiation and angiogenesis. *Cancer Res.* **66**, 9886-9894 (2006).
11. Richards, T.S. *et al.* Protein kinase C spatially and temporally regulates gap junctional communication during human wound repair via phosphorylation of connexin43 on serine368. *J. Cell Biol.* **167**, 555-562 (2004).
12. Yip, S.S. *et al.* Up-regulation of the protein tyrosine phosphatase SHP-1 in human breast cancer and correlation with GRB2 expression. *Int. J. Cancer*. **88**, 363-368 (2000).
13. van Adelsberg, J. Peptides from the PKD repeats of polycystin, the PKD1 gene product, modulate pattern formation in the developing kidney. *Dev. Genet.* **24**, 299-308 (1999).
14. Sohara, E. *et al.* Nek8 regulates the expression and localization of polycystin-1 and polycystin-2. *J. Am. Soc. Nephrol.* **19**, 469-476 (2008).
15. Kopfstein, L. & Christofori, G. Metastasis: cell-autonomous mechanisms versus contributions by the tumor microenvironment. *Cell. Mol. Life. Sci.* **63**, 449-468 (2006).
16. Haass, N.K., Smalley, K.S., Li, L. & Herlyn, M. Adhesion, migration and communication in melanocytes and melanoma. *Pigment. Cell Res.* **18**, 150-159 (2005).
17. Furman, C., Short, S.M., Subramanian, R.R., Zetter, B.R. & Roberts, T.M. DEF-1/ASAP1 is a GTPase-activating protein (GAP) for ARF1 that enhances cell motility through a GAP-dependent mechanism. *J. Biol. Chem.* **277**, 7962-7969 (2002).
18. Hildebrand, J.D., Taylor, J.M. & Parsons, J.T. An SH3 domain-containing GTPase-activating protein for Rho and Cdc42 associates with focal adhesion kinase. *Mol. Cell Biol.* **16**, 3169-3178 (1996).
19. Taylor, J.M., Macklem, M.M. & Parsons, J.T. Cytoskeletal changes induced by GRAF, the GTPase regulator associated with focal adhesion kinase, are mediated by Rho. *J. Cell Sci.* **112** (Pt 2), 231-242 (1999).
20. Shintani, T. *et al.* Eph receptors are negatively controlled by protein tyrosine phosphatase receptor type O. *Nat. Neurosci.* **9**, 761-769 (2006).
21. Vega, F.M. & Ridley, A.J. SnapShot: Rho family GTPases. *Cell*. **129**, 1430 (2007).
22. Fingar, D.C. & Blenis, J. Target of rapamycin (TOR): an integrator of nutrient and growth factor signals and coordinator of cell growth and cell cycle progression. *Oncogene*. **23**, 3151-3171 (2004).
23. Chang, L., Chiang, S.H. & Saltiel, A.R. Insulin signaling and the regulation of glucose transport. *Mol. Med.* **10**, 65-71 (2004).
24. Plas, D.R. & Thompson, C.B. Akt-dependent transformation: there is more to growth than just surviving. *Oncogene*. **24**, 7435-7442 (2005).
25. Cowin, P., Rowlands, T.M. & Hatsell, S.J. Cadherins and catenins in breast cancer. *Curr. Opin. Cell. Biol.* **17**, 499-508 (2005).

26. Ishizaki, Y. *et al.* Reduced expression and aberrant localization of p120catenin in human squamous cell carcinoma of the skin. *J. Dermatol. Sci.* **34**, 99-108 (2004).
27. Reynolds, A.B. & Rocznak-Ferguson, A. Emerging roles for p120-catenin in cell adhesion and cancer. *Oncogene.* **23**, 7947-7956 (2004).
28. Fuja, T.J., Lin, F., Osann, K.E. & Bryant, P.J. Somatic mutations and altered expression of the candidate tumor suppressors CSNK1 epsilon, DLG1, and EDD/hHYD in mammary ductal carcinoma. *Cancer Res.* **64**, 942-951 (2004).
29. Lee, M.J. & Stephenson, D.A. Recent developments in neurofibromatosis type 1. *Curr. Opin. Neurol.* **20**, 135-141 (2007).
30. Jacob, S.T. & Motiwala, T. Epigenetic regulation of protein tyrosine phosphatases: potential molecular targets for cancer therapy. *Cancer. Gene. Ther.* **12**, 665-672 (2005).
31. Bowers, A.J. & Boylan, J.F. Nek8, a NIMA family kinase member, is overexpressed in primary human breast tumors. *Gene.* **328**, 135-142 (2004).
32. Hennessy, B.T., Smith, D.L., Ram, P.T., Lu, Y. & Mills, G.B. Exploiting the PI3K/AKT pathway for cancer drug discovery. *Nat. Rev. Drug Discov.* **4**, 988-1004 (2005).
33. Boehm, J.S. *et al.* Integrative genomic approaches identify IKBKE as a breast cancer oncogene. *Cell.* **129**, 1065-1079 (2007).
34. Chen, H.Y. *et al.* A five-gene signature and clinical outcome in non-small-cell lung cancer. *N. Engl. J. Med.* **356**, 11-20 (2007).
35. Narayan, G. *et al.* Gene dosage alterations revealed by cDNA microarray analysis in cervical cancer: identification of candidate amplified and overexpressed genes. *Genes Chromosomes Cancer.* **46**, 373-384 (2007).
36. Bielenberg, D.R., Pettaway, C.A., Takashima, S. & Klagsbrun, M. Neuropilins in neoplasms: expression, regulation, and function. *Exp. Cell Res.* **312**, 584-593 (2006).
37. Zohrabian, V.M. *et al.* Gene expression profiling of metastatic brain cancer. *Oncol. Rep.* **18**, 321-328 (2007).